ISSN 1340-3745

ICRR

ICRR-Report-480-2001-10

Contribution to 27th International Cosmic Ray Conference (07 – 15 Aug. 2001, Hamburg) from Cosmic Ray Collaboration at Mt. Chacaltaya

(edited by A. Ohsawa)

INSTITUTE FOR COSMIC RAY RESEARCH
UNIVERSITY OF TOKYO

Content

Proceedings of ICRC 2001: 1 © Copernicus Gesellschaft 2001

ICRC 2001

The energy spectrum around the knee region observed at Mt. Chacaltaya

Honda,K.[1], Ohmori,N.[2], Shinozaki,K.[3], Inoue,N[3], Tamada,M.[4], Kawasumi,N.[1], Hashimoto,K.[1], Tsushima,I.[1], Ohsawa,A.[5], Aoki,H.[6], Yokoi,K.[7], Matano,T.[8], Martinic,N[9], Ticona,R.[9], and Aguirre,C.[9]

[1]Faculty of Engineering,Yamanashi University,Kofu,400-8511,Japan
[2]Faculty of Science,Kochi University,780-8520,Japan
[3]Faculty of Science,Saitama University,388-8570,Japan
[4]Faculty of Science and Technology,Kinki University,577-8520,Japan
[5]Institute for Cosmic Ray Research,University Tokyo,277-8582,Japan
[6]Faculty of Science,Souka University,192-8577,Japan
[7]College of science and Engineering,Japan
[8]Shibakubo-cho 3-28-10,Tanashi,188-0014 Japan
[9]Institute de Investigaciones Fisicas Universidad Mayor de San Andres,Bolivia

Abstract. Observation of EAS with the combination of emulsion chamber and EAS array is undergone at Mt.Chacaltaya. We report on the size spectrum of EAS observed in about 5 years and discuss the energy spectrum and composition in this spectrum range. The corresponding energy range is between 10^{14}eV and 10^{16}eV and includes the knee region. To discuss these characteristics ,detailed EAS simulations were fulfilled with the condition of arrangement of the array ,trigger and detector response. Specially,by the method of the different trigger efficiency between initiated low and high mass composition,the result of proton spectrum obtained at near 10^{14}eV is also reported.

1 Introduction

Explaining the knee region of the energy spectrum of the cosmic ray (CR) would shed light on CR origin and acceleration mechanism. But the possibility that the change of hadronic interaction at this energy range exists will puts some limits this speculation. For ground based array,the experimental observables which are measured in order to exact information about the energy spectrum are charged components of showers with density , muon , hadron detectors or $\check{C}$ erenkov detectors. Many experiments using the combined array of these detectors have been fulfilled to get the information of primary energy spectrum. However, the method to estimate the energy spectrum mainly depends on the assumed mass composition and simulated EAS developments through the atmosphere. Two fold assumption is hard to resolve clearly. Among these methods, it is simple method to estimate EAS size from the observation of low energy charged particles. Moreover, by choosing the observation altitude to be most effective to the development of EAS for the corresponding energy range of CR,one of the unsolved problem can be reduced. In our case,Chacaltaya altitude is fit to observe the maximum development of shower in the energy region $\sim 10^{15}$ eV and fluctuation of shower development is minimized. However, with only one station, we can not conclude the CR mass composition and spectrum in knee region. It is clear to combine results observed at different altitude which fits to observe some range of primary energy each other. Also, it is necessary observed values are comparable to each other directory. To this aim ,in this report we show the size spectrum observed at Mt. Chacaltaya altitude as an example.

Correspondence to: K.Honda(khonda@ms.yamanashi.ac.jp)

2 Experiment and Analysis

The combined experiment of a air shower array and an emulsion chamber at Mt. Chacaltaya (Bolivia, 5200m a.s.l., 540 g/cm^2 of atmospheric depth) was started from 1979. The array consists 45 scintillation detectors for measuring of charged particles (9 detectors of $1m^2$, 36 detectors of $0.25m^2$) and 13 fast-timing detectors(FT)for measuring the direction (5 detectors of $1m^2$, 8 detectors of $0.25m^2$) from 1991 as shown Fig.1. The array cover an area of radius 50m, a lot of detectors are concentrated to near the emulsion chamber room. All detectors are using with 5cm thickness of plastic scintil-

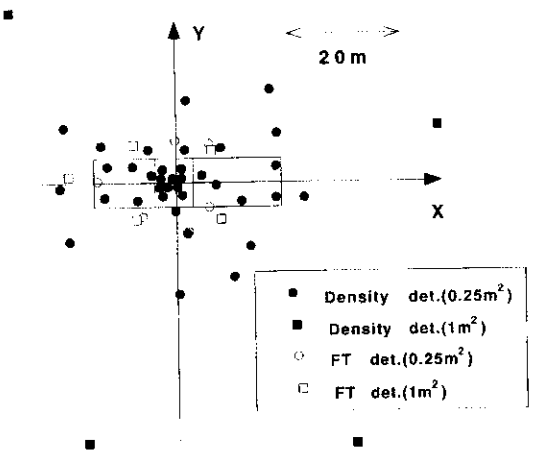

Fig. 1. The arrangement of our air shower array.

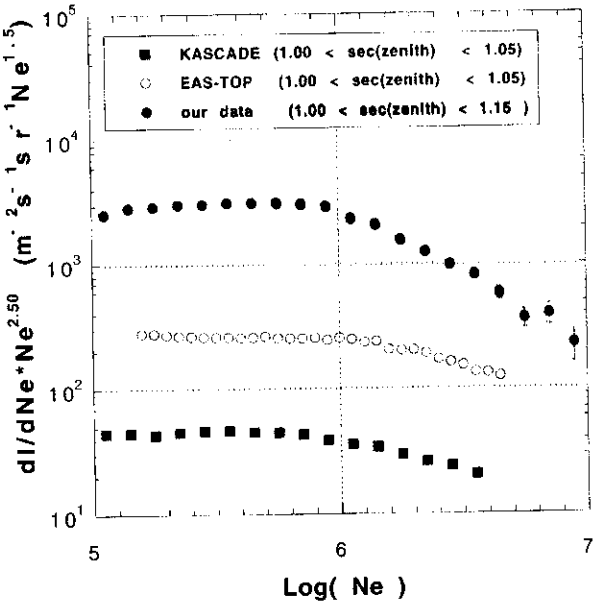

Fig. 2. Observed shower size spectrum is shown with closed circle. The shower size spectra of EAS-TOP(810 g/cm^2 and KASCADE(sea level) are shown in figure.

lator except 5 FT detectors with 10cm thickness. The recording system of the air shower is triggered above $\sim 10^4$ size [Kawasumi (1996)].

3 Results and Discussion

3.1 Size Spectrum

As explained in the experimental setups,using 45 scintillation counters and 13 FT detectors, incident angle and electron size of EAS were determined. The experiment for this analysis was carried out from 1992 to 1995. Total number of showers recorded is $\sim 3.3 \times 10^7$ in the effective observation time $\sim 7 \times 10^7$ seconds. The method to estimate the incident angle for each shower is ,using the all combination of 3 FT detectors to determine an incident angle , the most probable incident angle is obtained with the method of cluster analysis on these available combination of data. Compared with the EAS simulated FT data,the estimation errors of angle are lower than 3 degrees above the size range 10^4 . In the small shower size region, this method shows superiority to the usual least square method. For several scintillation counters show the fluctuation of the response (less than 20 %) in the observation period, corrections were applied with the statistical method for these detectors. Our array is not effective to observing lager size region. However, to arrange detectors compactly near the center of array and to limit analyzed showers whose shower axis hit within 6m radius from the center, showers to determine the size spectrum become more accurate in the smaller size region $\sim 10^5$. Observed shower size spectrum is shown in Fig. 2 with other size spectra observed at lower altitudes [Aglieta (1999)] ,[Castellina (2001)]

3.2 Energy Spectrum

The primary energy spectrum can be extracted from the measured electron size spectrum with informations of the mass composition and the relation between electron size and primary energy. In fact,the evaluated electron size spectrum is the convolution of the energy spectrum and a function describing the probability of a given primary to produce a shower with a certain size. With using EAS simulation,this relation between the electron size and the primary energy can be given. However, above probability function between size and energy depends not only on the EAS simulation code that describes EAS development in the atmosphere, but also on the response function characteristic to EAS array including detector response and the procedure to estimate the electron size from observed shower data.

The mass composition to investigate this knee region is not yet fixed even to use as the initial condition. So,avoiding the additive assumption,we have not used the assumption on mass composition. Moreover, primary mass is assumed to be proton only or to be iron only to the energy spectrum estimated for two extreme cases,. Followings are procedures to get the probability function we used. Simulation code is CORSIKA code with QGS Jet model. For each primary mass,about 10^5 events was simulated with energy above 2×10^4 GeV for proton primary and 5×10^4 GeV for iron primary. Simulated shower components were sampled to the real Chacaltaya EAS array and simulated the detector response for each detector (plastic scintillator with 0.25 m^2 area and 5 cm thickness) Those simulated EAS data were re-analyzed to get the size with the same procedure on the

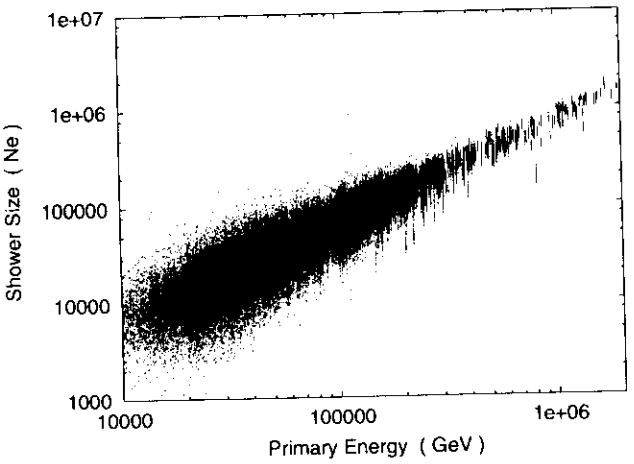

Fig. 3. Relation between Simulated primary energy and estimated shower size for proton . Trigger bias is included in this figure.

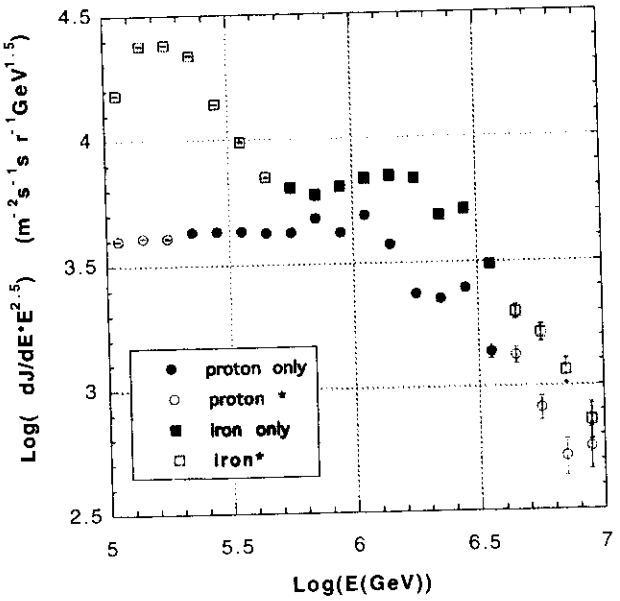

Fig. 4. Converted energy spectrum for proton and iron primary assumptions. circle is proton and square is iron primary. proton* and iron* in the figure mean the effect from the trigger bias for lower energy region, using the extrapolation for the high energy region.

same condition as explained section 3.1. .

For proton primary case,an example of the simulated size and energy relation is figured in Fig.3. The distribution profile of primary energy which results in a fixed size has a peak at the median, however the width of distribution is wide enough for a small size shower to contribute to the higher tail of energy spectrum. In the lower energy region is diffused by the trigger condition on the observability.

We tabulated probability function between size and energy,and converted observed electron size spectrum to an energy spectrum for each mass assumptions (proton only and iron only).

The converted energy spectrum is shown in Fig.4. In the energy range above Log(E(GeV))=6.6 for proton primary and iron primary shown with open circles and squares in this figure, the probability function to transform from size to energy was used with the extrapolated relation from the lower size and corresponding energy region shown with closed circles and squares. Because simulated number of showers is not enough to cover this energy range,but the energy distribution for fixed size has more sharp shape like a delta function. And as mentioned before, we used the tabulated probability distribution function, energy spectra for each composition show a little fluctuation on energy as seen. However, for iron component,the gross feature bumped in the energy range from 5.0 to 5.7 is the effect of the trigger condition,because in simulated shower initiated from iron primary shows the most effective trigger biases below the 5.7 region. and cannot be observed with such frequency. The effect of the trigger condition (at 90 % level) extends to the energy range below 5.3 for proton primary and 5.7 for iron primary. These effects are shown as different markings (open circles and squares) in the figure.

4 Conclusion

Our energy spectrum is re-display with overlapping other experimental results in Fig. 5 [Aglieta (1999)],[Amenomori (2000)], [Castellina (2001)] .

Below 5.7 in log energy scale,our energy spectrum only shows the case of lighter elements like proton dominated . In the energy region from 5.7 to 6.1, frequency difference between pure proton and iron is much small and has only 0.2 decade in this scale that corresponds to the difference ($\leq$ 50 %) in differential energy scale. Because in this energy region showers reach near the shower maximum at Mt. Chacaltaya altitude (540 g/cm^2) ,and the difference of shower development between these two primary masses is minimized. Above 6.1 in log energy scale, the frequency difference between proton primary and iron primary increase with energy and the imaginary turning point (knee) spreads from near 6.1 to 6.5 depending on the assumed mass composition. Comparing with other observed results, our data have relatively higher frequency than other experimental values. Especially in the energy region between 5.7 to 6.1 our data have relatively good reliance , but the difference is clear on the frequency. On this point,we can not exclude the possibility that produced some systematic difference with other experiments at this time.

Acknowledgements. I would like to thank staffs of Instituto de Investigaciones Physicas to keep the Loboratry at Mt. Chacaltaya.

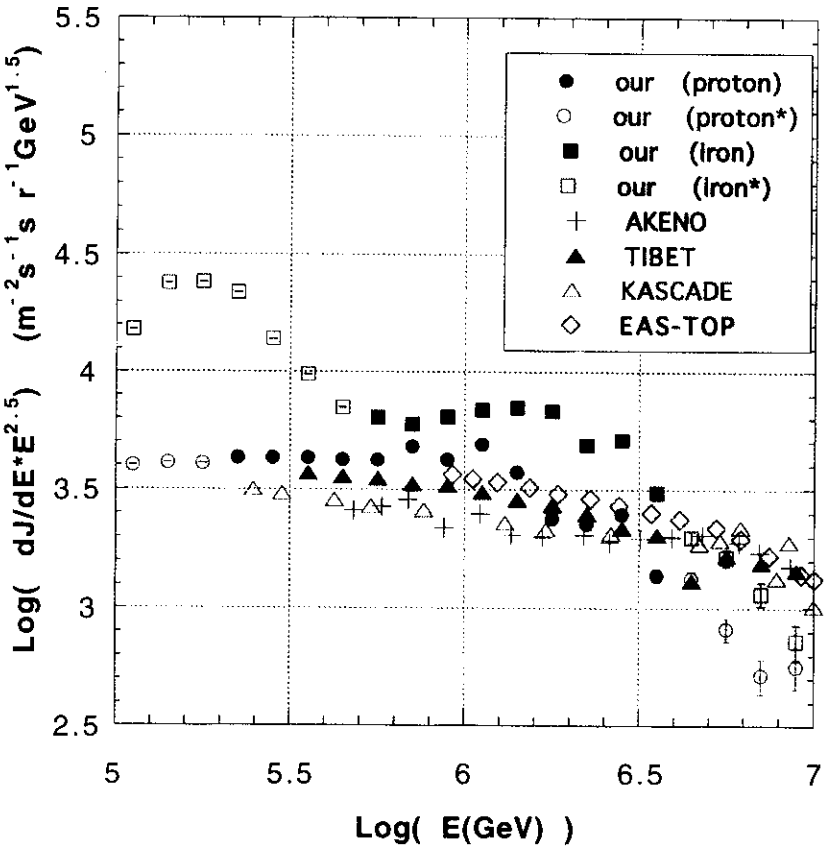

Fig. 5. Comparison between our energy spectra and other experiments .

References

N.Kawasumi et. al., Phys. Rev. D, 53, 3534–3546, 1996.
S.Petrera, IL Nuovo Cimento, 19, 737–754, 1996.
M.Aglietta et.al., Astroparticle Phys., 10, 1–9, 1999.
M.Amenomori et.al., Phys. Rev. D, 62, 112002-1–13, 2000.
A.Casrellina, Nuclear Physics B(Proc. Suppl.), 97, 35–47, 2001.

Proceedings of ICRC 2001: 1 © Copernicus Gesellschaft 2001

ICRC 2001

A Halo Event observed by Hybrid Detector at Mt. Chacaltaya

H. Aoki[1], K. Hashimoto[2], K. Honda[3], N. Inoue[4], N. Kawasumi[2], N. Martinic[5], C. Navia O.[6], N. Ohmori[7], A. Ohsawa[8], L. Oliveira C.[9], K. Shinozaki[4], M. Tamada[10], R. Ticona[5], and I. Tsushima[2]

[1]Faculty of Science, Soka University, Hachioji, Tokyo, 192-8577, Japan
[2]Faculty of Education, Yamanashi University, Kofu, 400-8510, Japan
[3]Faculty of Engineering, Yamanashi University, Kofu, 400-8511, Japan
[4]Faculty of Science, Saitama University, Urawa, 338-8570, Japan
[5]Instituto de Investigaciones Fisicas, Unversidad Mayor de San Andres, La Paz, Bolivia
[6]Departamento de Fisica, Universidade Federal Fluminense, Niteroi, Rio de Janeiro, RJ, Brasil
[7]Faculty of Science, Kochi University, Kochi, 780-8520, Japan
[8]Institute for Cosmic Ray Research, University of Tokyo, Kashiwa, 277-8582, Japan
[9]Centro Brasileiro de Pesquisas Fisicas, Rio de Janeiro, RJ, Brasil
[10]Faculty of Science and Technology, Kinki University, Higashi-Osaka, 577-8502, Japan

Abstract. Detailed description is made on a halo event which is obtained by the hybrid detector of an emulsion chamber and an air shower array at Mt. Chacaltaya (5,200 m, Bolivia). Available data for the event are on the halo ($E_{halo} \sim 750$ TeV) and on the high energy particles of electron/photon and hadronic components by the emulsion chamber, on low energy hadrons by the hadron calorimeter, and on characteristics of the accompanied air shower ($N_e \sim 7.0 \times 10^7$, $s \sim 0.59$) by the air shower array. Structure and origin of the event is discussed based on the observed data of various components.

1 Introduction

We have been observing high energy cosmic-ray events – air showers (AS) – by a hybrid apparatus of emulsion chamber (EC), air shower array and hadron calorimeter (HC) at Mt. Chacaltaya (5,200 m, Bolivia)[Kawasumi et al., (96); Aguirre et al., (00)].

We will report a high energy event which is remarkable by a large family with a halo (~ 1.5 cm of diameter) on X-ray films of EC. A halo is made of a large number of electrons, distributed continuously, which means high concentration of energy. The analysis of the halo which bears the information of air shower core helps us to understand the detailed structure of AS.

Correspondence to: Norio Kawasumi
(n-kawa@edu.yamanashi.ac.jp)

2 Description of the event

We will describe the event in relation to the respective detectors.

2.1 Air shower (AS) array

AS array consists of 39 plastic scintillator detectors which are distributed over a circular area of ~ 50 m radius. It can measure the arrival time and arrival direction of AS, together with the lateral distribution of charged particle density from which the age s and the total size N_e are estimated by fitting the lateral distribution to NKG function[Kamata and Nishimura, (58); Greisen, (58)]. We obtained $s \sim 0.59$ and $N_e \sim 7.03 \times 10^7$ for the present event. Hence the primary energy of AS is $\sim 1.5 \times 10^{17}$ eV approximately.

2.2 Hadron calorimeter (HC)

HC, located in the center of the AS array and placed beneath EC, consists of 32 plastic scintillators (0.25 m^2 each). It measures the arriving time of the event and the lateral distribution of charged particles which arrive at HC. These charged particles are mainly electrons which are produced by the hadrons incident upon EC, because electrons and photons, incident upon EC, are absorbed in EC of 15 cm Pb thick, equivalent to 30 c.u. or to 0.81 collision mean free path of nucleon. Therefore we can estimate the energy distribution of hadrons in AS from the lateral distribution of charged particle density

by HC[Aguirre et al., (00)].

That is, the lateral distribution is approximated as

$$n_b(r) = \frac{A}{{r_0}^2}(\frac{r}{r_0})^{-\alpha}$$

$$(r_0 = 1 \text{ m},\ A = 4.67 \times 10^5,\ \alpha = 2.89)$$

from which we can estimate the *differential* energy distribution of hadrons, incident upon EC, as

$$n_h = \left(\frac{dN_h}{dE}\right)_{E=1\text{TeV}} = 3.54 \times 10^3 \quad (/1 \text{ TeV})$$

and the power index $\alpha - 4 = -1.1$ in the energy region $E = 0.1 \sim 1$ TeV. (See Fig. 5.)

2.3 Emulsion chamber (EC)

32 EC's of 15 cm Pb thick and 0.25 m^2 each, placed on HC, have 14 sensitive layers of X-ray films which are inserted at every 1 cm of Pb plate.

The event on the X-ray film consists of several tens of showers, distributed over the area of ~ 10 cm radius, and of a halo of diameter ~ 1.5 cm in the center of the event.

The event hit the upper-left corner of the EC unit No.3 with inclination $\sim 10°$. Therefore a part of particles fell outside EC, and the halo in the center of the event leaves EC at large depth (after 12 cm Pb).

In this sense shower detection is biased by the following two reasons.

1. The halo masks the showers.
2. The event hit the upper-left corner of EC unit.

which are called 'the item 1' and 'the item 2' hereafter. The item 1 is discussed in the subsection 3.1, and the item 2 is corrected by sampling the showers only in the third quadrant (*i.e.* $\varphi = 270° \sim 360°$) of the xy coordinates whose origin is located at the center of the halo, and by multiplying the number by 4.

3 Halo and showers by the emulsion chamber

3.1 Halo

The opacity of the halo on X-ray film is measured by a microphotometer (with the slit of 200×200 μm^2) over the square area of 1 cm $\times$ 1 cm at 500 μm interval. The opacity D, called 'darkness', is converted to electron density ρ_e using the $\rho_e - D$ relation, obtained beforehand. In this way we obtain the lateral distribution of electron density $\rho(r,t)$ at every depth t in EC.

(1) Transition curve of the total electron number

Fig. 1 shows the transition curve of the total electron number in the halo, which is obtained by the integration

$$N_e(t) = \int_0^{r_{th}} \rho(r,t) 2\pi r dr$$

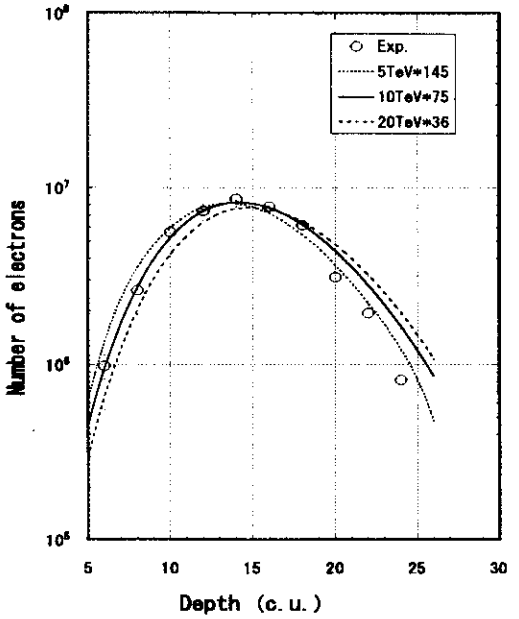

Fig. 1. Transition curve of the total electron number. The total electron number is obtained by integrating the lateral distribution of the electron density, which is obtained from the local darkness in the halo, at every sensitive layers in EC. The curves are those which are produced by N_γ γ-rays with energy $< E >$, tabulated in Table 1, incident upon EC.

where r_{th} is the distance at which the darkness is the threshold darkness $D_{th} = 0.1$.

We assume that the halo is produced by a bundle of high energy γ-rays in the air shower.[1] Then, according to the cascade theory[Nishimura, (67)], the maximum depth t_{max} of the transition curve of the halo is given by

$$\ln \frac{< E >}{\epsilon} = \lambda_1'(s) t_{max} \simeq t_{max}$$

where $\epsilon = 7.4$ MeV is the critical energy of Pb and $< E >$ is the average energy of γ-rays, incident upon EC. Since $t_{max} \simeq 14$ c.u., we have $< E >= 8.9$ TeV. Three curves in Fig. 1 are the transition curves of total

Table 1. Energy and number of γ-rays, incident upon EC, to produce the halo.

$< E >$ (TeV)	N_γ	E_{halo} (TeV)
5	145	725
10	75	750
20	36	720

[1] Strictly speaking, photons and electrons. We will refer to them as γ-rays, following the EC terminology.

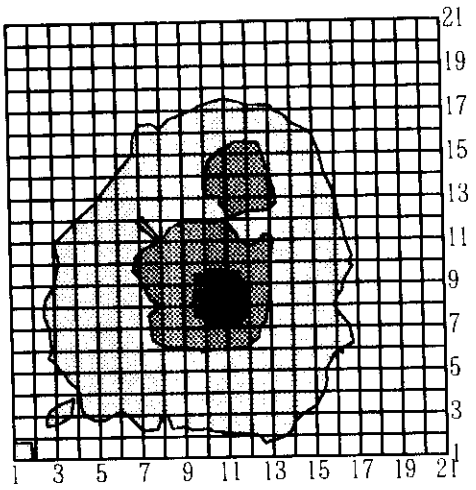

Fig. 2. The contour map (1 div. = 500 μm) of the darkness D in the halo at the depth 14 c.u., where the total number of electrons attains the maximum development approximately. The steps of the contours are $D = 0 \sim 1.0$, $1.0 \sim 2.0$, ...

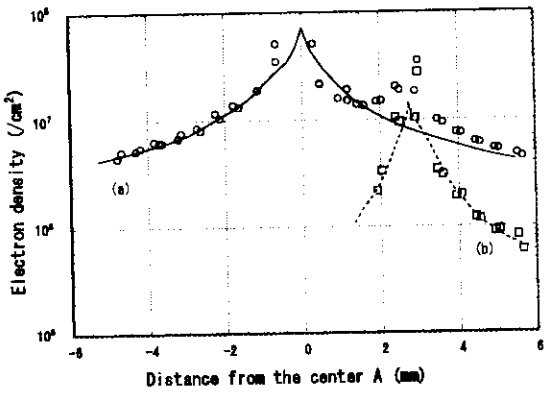

Fig. 3. Lateral distribution of electron density along the line to connect the cores A and B. Circles are the experimental data and the squares are after subtraction of the curve (a) which is the best-fit to the data points of the core A.

electron number for the cases in Table 1. Fig. 1 shows that the case of $< E >= 10$ TeV describes the data best among the three, giving the total observed energy 750 TeV in the halo.

We try to estimate the energy spectrum of γ-rays, incident upon EC, from $< E >= 10$ TeV and $N_\gamma = 75$ the transition curve of which gives the best-fit to the experimental data. Assuming the energy spectrum as

$$N_0\gamma\left(\frac{E}{E_{th}}\right)^{-\gamma-1} d\left(\frac{E}{E_{th}}\right), \qquad (1)$$

we have

$$< E >= \frac{\gamma}{\gamma-1}E_{th} \qquad \text{and} \qquad N_\gamma = N_0\ ,$$

where N_0 is the number of γ-rays at $E = E_{th}$. That is, if we assume the exponent γ, we can obtain the energy spectrum which is tabulated in Table 2.

The energy spectra of γ-rays for the cases in Table 2 are shown in Fig. 4, together with experimental data of γ-rays found outside the halo. We consider that the latter spectrum is biased due to the masking by the halo but is not biased seriously in the low energy region. Consequently we have a conclusion in Fig. 4 that the case of $\gamma = 1.75$ in Table 2 is the best among the three.

Table 2. Energy spectrum of γ-rays to produce the halo

γ	E_{th} (TeV)	N_0
2.0	5.0	75
1.75	4.3	75
1.5	3.3	75

(2) Lateral distribution of the halo

The contour map of the darkness D in the halo (Fig. 2) shows that the halo contains two high energy cores, A and B (with A > B). Fig. 3 shows the lateral distribution of the electron density along the line to connect A and B, at the depth of 14 c.u. where the total number of electron attains the maximum development approximately. The curves (a) and (b) in Fig. 3 are the best-fit to the data points, assuming that the distribution is symmetric around the core center. The maximum values of the distribution for A and B are used to estimate the energies of the cores A and B, which are tabulated in Table 3.

It is worthy mentioning that the assumed lateral distributions appear to be wider than that of the electron density in the cascade theory. But quantitative discussion is not easy because the observed region is quite limited, compared with 1 Moliere unit 1.62 cm.

3.2 Individual showers

Several tens of γ- and hadron-origin showers are distributed over an area of $r \sim 10$ cm. Routine process of EC measurement gives shower energies and shower starting points Δt for respective showers. Showers with $\Delta t > 6$ c.u. are defined as those of hadron-origin and the rest those of γ-origin. By this definition 15 % of

Table 3. The estimated energies of the cores in the halo

Core	Electron density at the core center (/cm^2)	Energy (TeV)
A	7.3×10^7	640
B	1.3×10^7	110
Total		750

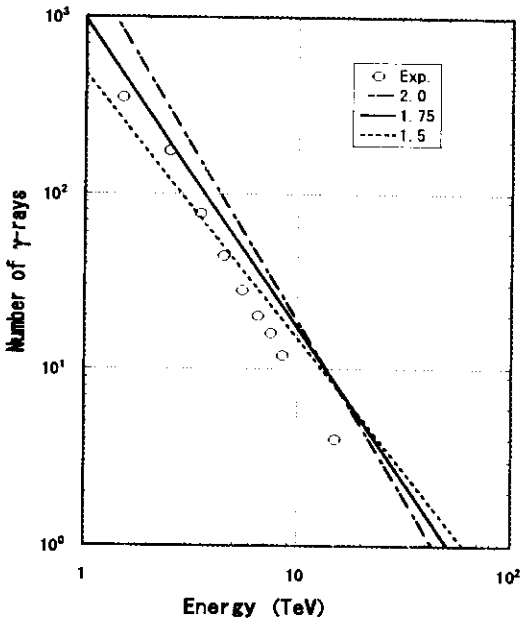

Fig. 4. Energy spectrum of γ-rays which are found outside the halo (corrected for the item 2). The lines are those which are assumed to produce the halo. (See Table 2.)

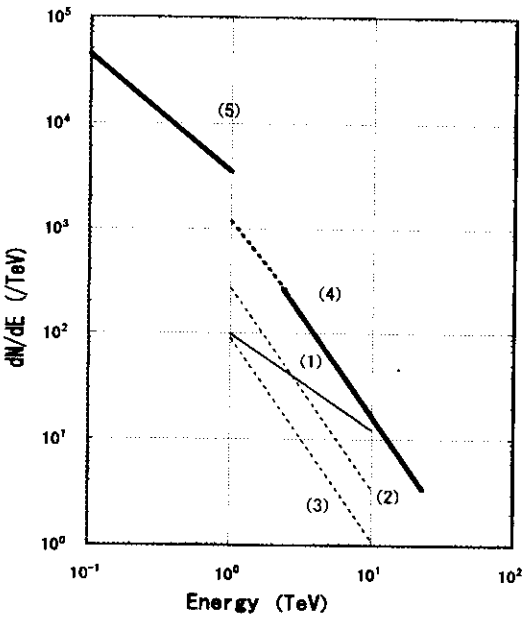

Fig. 5. Differential energy spectrum of hadrons; the line (4) by EC (corrected for the item 1) and the line (5) by HC.

The line (1) is the integral energy spectrum of hadron-induced showers by EC, and the line (2) is the differential. Then corrections are made for the collision probability of hadrons (the line (3)) and for the conversion of observed energy to hadron energy k_γ (the line (4)). That is, $E_{ob} = k_\gamma E_h$ with $< k_\gamma >= 1/6$.

the hadron-origin showers are mixed up among γ-origin showers.

Fig. 4 shows the energy spectrum of γ-rays which are found outside the halo (*i.e.* $r \geq 0.8$ cm). The number of γ-rays is corrected for the item 2, but the spectrum is still biased due to the item 1. The solid line is the estimated one from the halo characteristics.

Fig. 5 shows the differential energy spectrum of the hadron-origin showers, which are found outside the halo by EC (the line (4)), together with that which is estimated from the data by HC (the line (5)). Consistency of both spectra may indicate that the event represents the average character of AS development without serious fluctuation.

4 Summary

We analyzed a high energy event with a halo.
(1) The accompanying air shower has the age $s = 0.59$ and the size $N_e = 7.03 \times 10^7$.
(2) The halo is produced by γ-rays with the total energy 750 TeV, which has the energy spectrum of eq.(1) with $\gamma = 1.75$ and $N_0 = 75$. The energy spectrum is consistent with that of γ-rays which are observed outside the halo.
(3) The two energy spectra of the hadron component in AS, by EC and by HC, are consistent with each other.

Following points will be discussed elsewhere.

(1) Lateral distributions of γ-rays and hadrons.
(1) How the events is observed at the sea level ?
(2) Can a conventional model of hadron interactions produce the event ?

References

N. Kawasumi et al., Phys Rev. D, Vol. 53, 3534-3546, 1996.
C. Aguirre et al., Phys. Rev. D, Vol. 62, 032003-1-17, 2000.
K. Kamata and J. Nishimura, Prog. Theor. Phys. Suppl., 6, 93,1958.
K. Greisen, Progress in Cosmic Ray Physics(North-Holland, Amsterdam), Vol. 3, 1958.
J. Nishimura, Handbuch der Physik(Springer, Berlin), Vol. 46/2, 1967.

Proceedings of ICRC 2001: 1–4 © Copernicus Gesellschaft 2001

ICRC 2001

Forbush Decreases in a Year of 2000 Observed by Air Shower Detectors at Mt.Chacaltaya

A.Mahrous[1], N.Inoue[1], K.Shinozaki[1], Y.Takahashi[1], K.Miyazawa[1], K.Honda[2], N.Kawasumi[3], I.Tsushima[3], K.Hashimoto[3], A.Ohsawa[4], N.Ohmori[5], M.Tamada[6], H.Aoki[7], N.Martinic[8], R.Ticona[8], C.Aguirre[8], F.Osco[8], N.Huayhun[8], and R.Gutierrez[8]

[1]Department of Physics, Saitama University, Urawa, Saitama, Japan
[2]Faculty of Engineering, Yamanashi University, Kofu, Japan
[3]Faculty of Education, Yamanashi University, Kofu, Japan
[4]Institute for Cosmic Ray Research, University of Tokyo, Kashiwa, Chiba, Japan
[5]Department of Physics, Kochi University, Kochi, Japan
[6]Faculty of Science and Engineering, Kinki University, Ohsaka, Japan
[7]Faculty of Engineering, Souka University, Tachikawa, Tokyo, Japan
[8]Instituto de Investigaciones Fisicas, Universidad Mayor de San Andres, La Paz, Bolivia

Abstract. Forbush decreases have been detected by unshielded and shielded air shower detectors at Mt.Chacaltaya in June , July and November of 2000. The deficits of cosmic ray counting rates were recorded ones of 3% – 6% in each event. While a time structure of deficit in June gives a simple feature, one in July has rather complicated structure in the stage of decrease and also in a period of recovering of counting rate. Characteristics of Forbush decreases are introduced and discussed on it together with the information of neutron monitor located at Mt.Chacaltaya.

1 Introduction

Solar flares accompanied with CME(Coronal Mass Ejection) have been reported in June, July and November of 2000 as listed below,
A:11h25mUT of June 06(51701.47569MJD) X2.0/3B
B:14h18mUT of June 23(51718.59583MJD) M3.0/1F
C:21h05mUT of July 10(51735.87847MJD) M5.7/2B
D:18h47mUT of July 11(51736.78264MJD) M1.1/1N
E:10h18mUT of July 12(51737.42916MJD) X1.9/2B
F:10h03mUT of July 14(51739.41875MJD) X5.7/3B
G:06h45mUT of July 19(51744.28125MJD) M6.4/3N
H:11h17mUT of July 22(51747.47014MJD) M3.7/2N
I:02h43mUT of July 25(51750.11319MJD) M8.0/2B
J:05h34mUT of Nov. 23(51871.23194MJD) C5.4/1F
K:21h00mUT of Nov. 25(51873.87500MJD) X1.0/2N
Forbush decrease has been considered as a deficit of galactic cosmic ray intensity due to the CME cloud which is produced by a reconnection of solar magnetic field associated with a big solar flare. A deficit of intensity is due to the passage of condensed and irregular magnetized shock with a velocity of $\sim$1000kms^{-1} and the magnetic shield effect after the passage. The time structure of deficit, in general, shows a quick decrease of cosmic ray intensity in an order of hours when CME arrives. Then, an intensity becomes increase slowly with a recovering time of 1 or 2 weeks. This profile is not commonly formalized as a simple shape and sometimes shows complicated feature(ie.Wibberenz,1997). It has to be affected by a size, a velocity and a strength of irregular magnetic field of CME and associated shock wave. A report suggested a pre-cursory decrease which happened preceded the Forbush decrease(Morishita,1997). This is also one of unsolved phenomena.

Correspondence to: N.Inoue (Email:ninoue@post.saitama-u.ac.jp)

2 Experimental

Air Shower array and Emulsion Chamber experiment at Mt.Chacaltaya (AS-EC Experiment at 5200m a.s.l) has been carried out from 1979 to study the chemical composition of primary cosmic ray and high energy particle interaction in an energy region of 10^{14}eV–10^{17}eV(Kawasumi, 1996).

Air shower array consists of 40 and 4 unshielded scintillation detectors (N-detectors) with an area of $0.25m^2$ and of $1.0m^2$, respectively, to determine a lateral distribution of charged particles in an air shower as shown in fig.1(upper). 8 and 5 fast timing scintillation detectors(FT-detectors) with an area of $0.25m^2$ and of $1.0m^2$ are located in a central region of air shower array to determine an arrival direction of air shower. In addition, $8m^2$ hadron detector which consists of 32 shielded scintillation detectors(B-detectors) with an area of $0.25m^2$ is used for the detection of high energy hadronic component in air shower core as shown in fig.1(lower). Each B-detector is covered with 15cm thickness lead plate(30 c.u.) and it can detect muon component with a threshold energy of 0.34GeV for vertical incident one. Signals of background secondary particle produced by primary galactic cosmic rays from N and B detector are monitored independently and continuously. An integrated number of cosmic ray particles is recorded in every 10 seconds interval.

Signal of N-detector is considered to be caused by a pas-

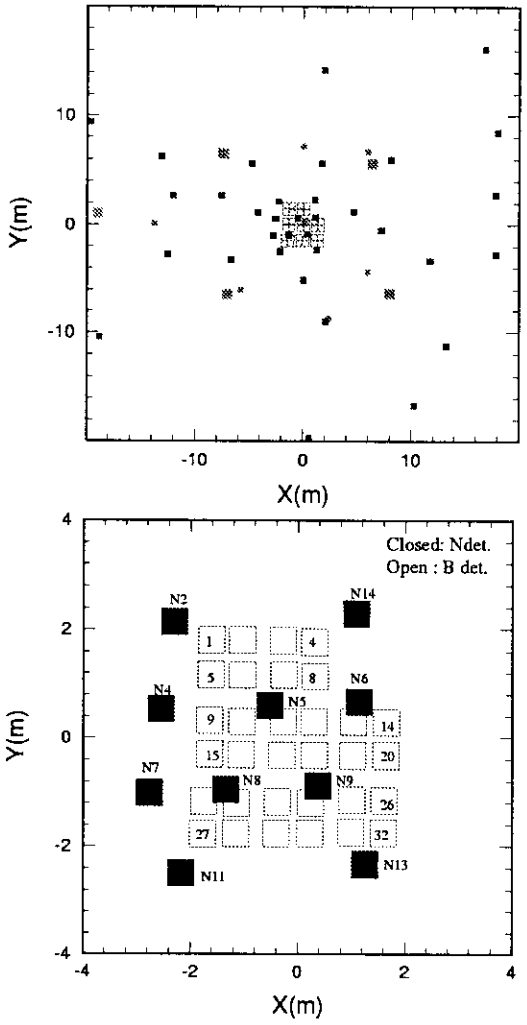

Fig. 1. Air shower array at Mt.Chacaltaya. N and FT detectors are shown by small squares and closed circles, respectively(in top figures). $8m^2$ hadron detector is located in a center of air shower array and positions of B-detectors are drawn by open squares together with some N-detectors in a bottom figure.

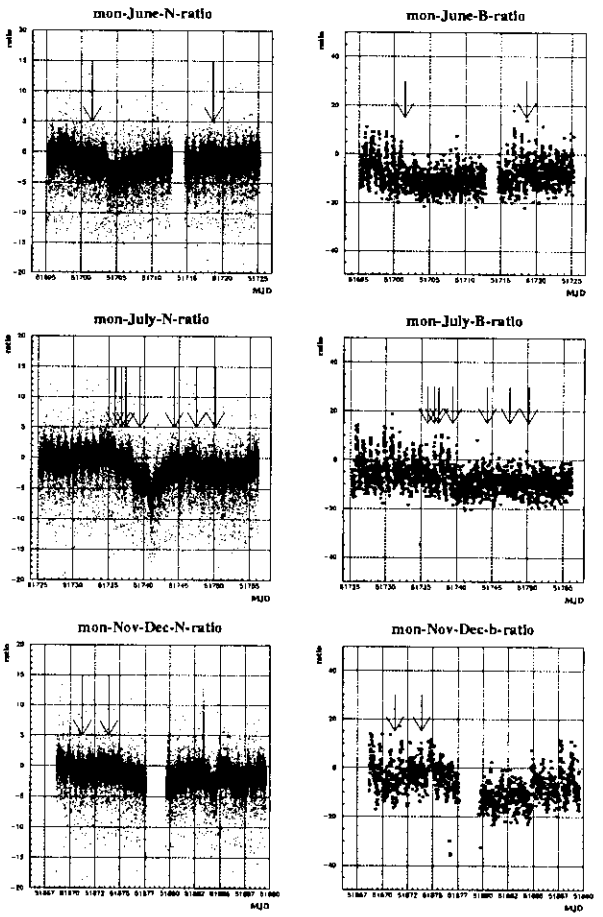

Fig. 2. Forbush decreases in June, July and November of 2000 are shown. Three upper figures show cosmic ray counting rates (a sum of all N-detectors) as a function of MJD. Three lower ones show cosmic ray counting rate (a sum of all B-detectors). Its counting rate is defined as a deviation in % from the average. Times of solar flares are shown by the arrows in each figure.

sage of secondary electromagnetic particles(electrons and gamma-rays) and muons component produced by primary galactic proton. At higher altitude, electromagnetic component is not enough absorbed in the atmosphere, and a contribution to output signal of electromagnetic particles still appears as 45% of the numbers of signals from a simulation. Furthermore, signal of B-detector is mainly produced by muon component with an energy greater than 0.34GeV. A mode energy of primary cosmic ray which gives a signal at the ground is roughly estimated as ~60GeV and ~70GeV for recorded particles by N and B-detectors from a response function taking into account of an effect of geomagnetic field at this geometrical location(a longitude, a latitude and a height of the site) and the detector characteristics. 12NM64(super neutron monitor) has been also operated in air shower array for monitoring the solar neutron and it has observed the neutron intensity in every 1 minute with an information of atmospheric pressure at the site. Time variations of cosmic ray counting rate listed below, have not made any corrections on effects of an atmospheric pressure, a temperature and a daily modulation of galactic cosmic rays.

3 Results and Discussion

In fig.2, events of Forbush decreases in June, July and November of 2000 are shown. Three left figures show cosmic ray counting rate (a sum of all N-detectors) as a function of MJD. A counting rate is defined as a deviation in % from the average counting rate. Three right figures show ones from a sum of all B-detectors. Times of solar flares listed before are indicated by arrows in each figure. The maximum deficit of cosmic ray intensity observed by N-detectors is 3.8% and 5.5% for events in June and July, respectively. A time structure of deficit observed in June has rather simple form, but one in July seems to have a characteristic feature with two

steps structure in a stage of decrease and a longer recovering time of 15 – 20days after a time of the minimum deficit. Deficits in data observed by B-detectors also show somewhat larger values of 6% and 6.5% for events in June and July. Another feature in the deficit is a smaller amplitude of periodic variation of cosmic ray counting rate around a period of Forbush decrease. An amplitude of periodic variation suddenly decreased and became to nearly a half of usual one . Then, it became to the usual amplitude when Forbush decrease finished. This profile can be also seen in a time variation of N-detectors with smaller changes.

Fig.3 shows detail time variations of counting rate in 10 days around solar flares of June and July. Top figures are cosmic ray counting rate from N-detectors in a period of June 5 – June 15 and July 10 – July 20. Results of Forbush decreases from 12NM64 are given in the second column. A counting rate of neutrons in every 1 minute is shown in a vertical axis. Results of Forbush decrease detected by NORIKURA Muon Telescope are also shown in the bottom figures(private communication). Times of solar flares in this periods are shown by arrows with a magnitude of solar flare in optical measurement in these figures. Profiles of time structures observed by three different equipments and at different location of Japan and Bolivia are likely to be consistent with each other. There is a complex structure in Forbush decrease of July. This is a reason of the contributions of seven solar flares with CME occurred in a short period of July. This time structure which seems to be affected by a physical structure of magnetic field in a shock created by high velocity shock fronts, CMEs and also by magnetic barrier caused by outgoing CMEs. A time structure in a stage of intensity recovering dose not show a simple one and has presented a longer effect. This fact suggests that a structure of magnetic field in outgoing shocks was not static and has strong irregularity exceed to one of typical structure.

There can be seen that neutron counting rate observed by 12NM64 has a periodic variation of $\sim$12 hours. This feature can be explained by a 12-hours variation of atmospheric pressure caused by a tide-generating force by the sun. Atmospheric pressure variations recorded at Mt.Chacaltaya are shown in the third column of the figures. A half day atmospheric pressure variation has been observed with an amplitude of $\pm$0.6[hPa] at Mt.Chacaltaya. According to a simulation, this variation promises to give a contribution of $\pm$0.45% in a total amplitude of variation. An amplitude of a half day variation in experimental neutron counting rate in the figures is almost consistent with this expectation. Periodic variations in profiles observed by N and B-detectors can be also seen and show a lager amplitude in comparison with one of neutrons. This is considered as a result of overlapped contribution of 12 hours atmospheric pressure variation, a temperature effect to the detector and a daily modulation of galactic cosmic rays. It is easy to suppose that an effect of temperature variation has to be dominant because a temperature control to air shower detectors has not performed for air shower detectors. However, if the fact that a decrease of amplitude of periodic variation in a period of Forbush decrease mentioned before is significant, an explanation for a decrease of amplitude has to be seek in a global physical effect belong to a flow of galactic cosmic rays outside of atmosphere. Definite answer to this question is still open, but it is required to make a continuous examination.

Our air shower array has been observed air showers and the numbers of air showers has been analyzed in such period of Forbush decreases. The numbers of showers with zenith angles less than 44° and Ne greater than 10^4, which corresponds to an primary energy of 30TeV at Mt.Chacaltaya, are shown in a top(June) and a bottom(July) of fig.4. No significant deficit of the number of air showers in such period could be seen. This shows an intensity of magnetic field and structure around the earth dose not give an effect for galactic cosmic rays with such energies even in a time of solar flare.

We have not made a detail discussion on the Forbush decrease in November because of lacks of N(and B) detectors data in some days during a period of Forbush decrease. However a time structure of deficit seems to be almost same with one recorded in June. Another event in March 2001 has been already recorded in our data and more statistics will be expected in a couple of year. Detail experimental analysis will be done after making corrections for effects of atmospheric pressure and temperature on the counting rate of N(and B) detectors, and then characteristics of deficit has to be examined for existed and next coming Forbush decrease. Any simulation of a time structure of deficit will be also requested with assumptions of temporal structure of CME shock wave to explain the experimental characteristics.

Acknowledgements. The authors wish to express their gratitude to the financial support by the Society for the Promotion of Science, which made it possible to realize this international collaboration. This experiment was also supported partly by Science Research Funds of Ministry of Education, Science and Culture in Japan, by the Institute for Cosmic Ray Research, University of Tokyo. The authors are indebted to the Bolivian staff of Cosmic Ray Laboratory at Mt.Chacaltaya.

References

Kawasumi,N., Tsushima,I., Honda,K. et al. ,*1996, Phys. Rev. D*, **D53**, 3534

Morishita,I., Fujimoto,K., Fujii,Z., et al. ,*1997, Proc. Inter. Cosmic Ray Conf.*, **1**, 405

Wibberenz,G., Cane,H.V. and Richardcon, I.G. ,*1997, Proc. Inter. Cosmic Ray Conf.*, **1**, 397

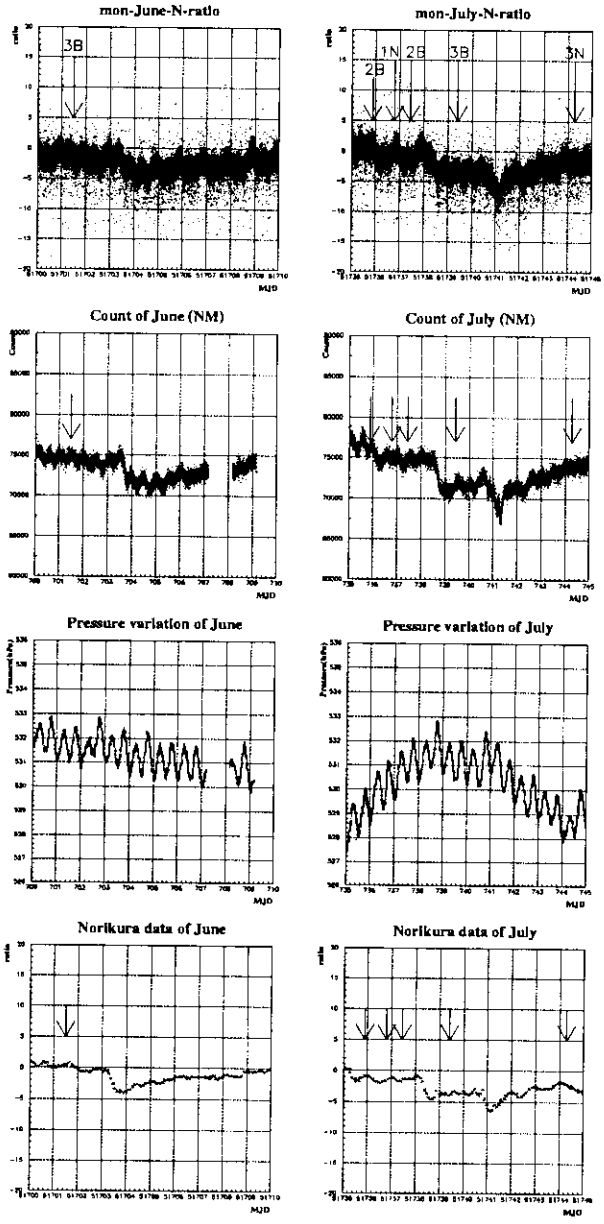

Fig. 3. Counting rate variations in 10 days around solar flares of June and July. Top figures are cosmic ray counting rate of N-detectors in a period of June 5 – June 15 and July 10 – July 20. Forbush decrease detected by 12NM64 in June and July are also given in the second column of the figures. Atmospheric pressure variations in the same periods are shown in the third column. Results of Forbush decreases observed at NORIKURA Muon Telescope are shown in the bottom figures.

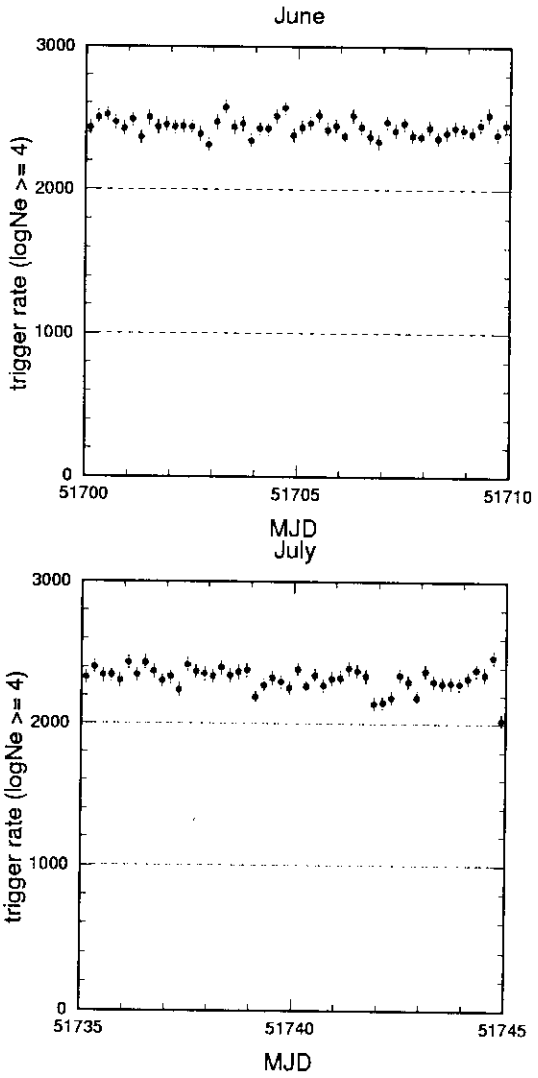

Fig. 4. The numbers of showers with Ne greater than 10^4 and zenith angle less than 44°. Results of June and July are shown in a top and a bottom figure, respectively.

Proceedings of ICRC 2001: 1 © Copernicus Gesellschaft 2001

ICRC 2001

ALGORITHMS BASED ON ISOTROPIC AZIMUTHAL ANGLE DISTRIBUTION OF INTERACTION SECONDARIES

C.R.A.AUGUSTO[1], S.L.C.BARROSO[2], P.C.BEGGIO[3], A.O.CARVALHO[2], M.J.MENON[2], C.E.NAVIA[1], R.OLIVEIRA[2], and E.H.SHIBUYA (BRAZIL-JAPAN COLLABORATION OF CHACALTAYA EMULSION CHAMBER EXPERIMENT)[2]

[1]Instituto de Física, Universidade Federal Fluminense, 24210-130 Niterói, RJ, Brazil
[2]Instituto de Física 'Gleb Wataghin', Universidade Estadual de Campinas, 13083-970 Campinas, SP, Brazil
[3]Laboratório de Ciências Matemáticas, Universidade Estadual do Norte Fluminense, Campos dos Goytacazes, RJ, Brazil

Abstract. An azimuthal angle distribution of events measured by Brazil-Japan Chacaltaya Emulsion Chamber Experiment (B-J Collaboration) shows that the secondaries produced by cosmic ray interaction particle are isotropic. Algorithms based on these observations were analytically calculated and their application to near 372 interaction events will be presented. One of these algorithms is equivalent to Duller-Walker plot High-Energy Meson Production. Duller and Walker (1954) and therefore it is possible to anlyse the events as having structure of jet emission, through tests of their 'sphericity'. From the distribution of this ad-hoc defined sphericity it is possible to infer about the jet structure. Another apropriate combination of the calculated moments is used to get insights of superposition of interactions and/or production of more than one jet simultaneously.

1 Introduction

A series of detectors called emulsion chambers (for instance in Fire-Balls in Pion Multiple Production. B-J Collaboration (1983)) have been exposed to Cosmic Rays incident on the Observatory of Mount Chacaltaya (5220 m above sea level and 20 km far from La Paz City, Bolivia) by B-J Collaboration, since 1962. The geographic coordinates of this Observatory are: $16^0 20' 45''$ South and $68^0 07' 31''$ West, which corresponds to geomagnetic coordinates $4^0 50' 40''$ South and $0^0 50' 20''$ East, respectively. These exposures observe secondaries of hadronic interactions as black spots in X-ray films and clusters of electron tracks in emulsion plates, both photosensitive material composing the detector. Lead plates are inserted between the envelopes containing photosensitive material, working either as a eletromagnetic particles converter or as a target for hadronic interaction particles. Then, the sensitive material of the detector always registers groups of electromagnetic tracks.

Correspondence to: E.H.Shibuya(shibuya@ifi.unicamp.br)

2 Description of experiment and method

A typical emulsion chamber is constituted by an upper chamber over blocks of compacted plastic sheets or asphalt pitch, both located on a iron frame platform and below those, an lower detector spaced by an air gap. The analysis was done in a sample of 372 events, where 87 events are observed only in the lower detetor, then these events are called C-jets. Other 285 events, called A-jets, were observed since the upper detector. Included in these A-jets sample there are 5 unusual events, Centauro events, analysed in two other contributions for the conference.
Beyond a traditional analysis done in some occasions, here we suggest a method based on an azimuthal isotropic decay of secondaries observed in figure 1. The superposed experimental distributions for A-jets and C-jets were compared with a uniform distribution and resulted in reduced χ^2 values between 1.1 and 1.8.

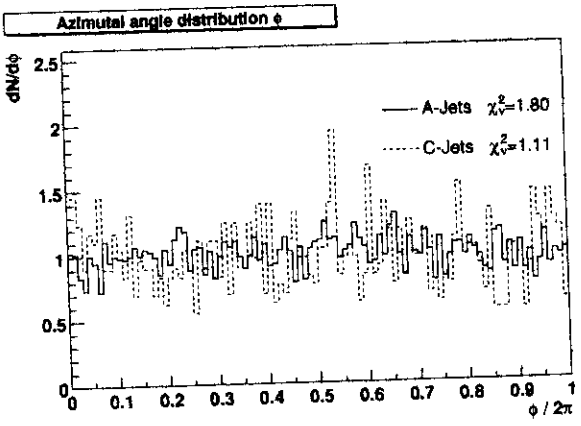

Fig. 1. Azimuthal angle distribution

Based on this observed isotropic azimuthal angle distribution, the secondary particles distribution composed by energy E^* and solid angle Ω^*, expressed in a center of mass system,

$$dN = g(E^*, \Omega^*) dE^* d\Omega^* \quad (1)$$

transforms in a general expression for the moments below, where E_i and θ are the energy and zenital angle of i^{th} particle, n is the order of moment, Γ and M are the Lorentz factor and Invariant Mass of the group of particles, respectively.

$$\Sigma E_i(\Gamma\theta_i)^n \simeq M\Gamma \int_{\frac{1-\Gamma^2\theta^2}{1+\Gamma^2\theta^2}}^{1} \frac{(1-x^2)^{\frac{n}{2}}}{2(1+x)^{n-1}} dx \qquad (2)$$

All the moments are functions of $\Gamma\theta$ and so, functions of $r/\bar{r}$, where $\bar{r}$ is related to Lorentz factor and H(interaction height) through $\Gamma = \bar{r}/H$. Therefore, the algorithms are useable even for events without height determined.

Taking the 0^{th}, 1^{st}, 2^{nd} and 3^{rd}, a proper combination of them, each one normalized, it were constructed algorithms called R and mDW. The first one, R, is defined as a ratio as follows:

$$R = \frac{[\Sigma E_i][\Sigma E_i(\Gamma\theta_i)^2]}{[\frac{4}{\pi}\Sigma E_i(\Gamma\theta_i)]^2} \qquad (3)$$

where both, the numerator and denominator, are functions of $\Gamma\theta$ and of squared Invariant Mass as could be seen in the appendix. So, the events that fits this analytical curve are events coming from one jet produced at one single interaction point. Examples of application of algorithm R are presented in figures 2 and 3 for C-jet and A-jet, respectively. This algorithm was firstly used in Indication of η-meson production in gamma-ray families. Shibuya (1983) to present production of mesons heavier than π^0 mesons.

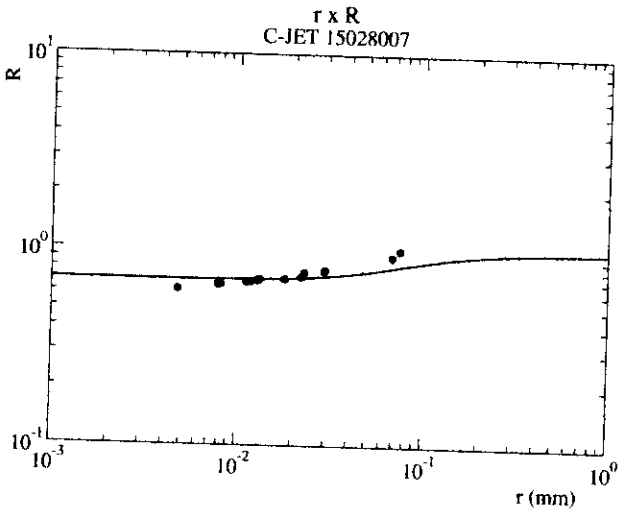

Fig. 2. Example of algorithm R for C-jet

The second algorithm was called mDW due to its similarity to the Duller-Walker plot (High-Energy Meson Production. Duller and Walker (1954)), used to show the sphericity of a jet. It differs from that in the fact that it uses also the energy of each member of a jet and does not necessary to know the total multiplicity, a priori. The events that fits this curve are interpretable as spherical because the slope is 2, same kind of

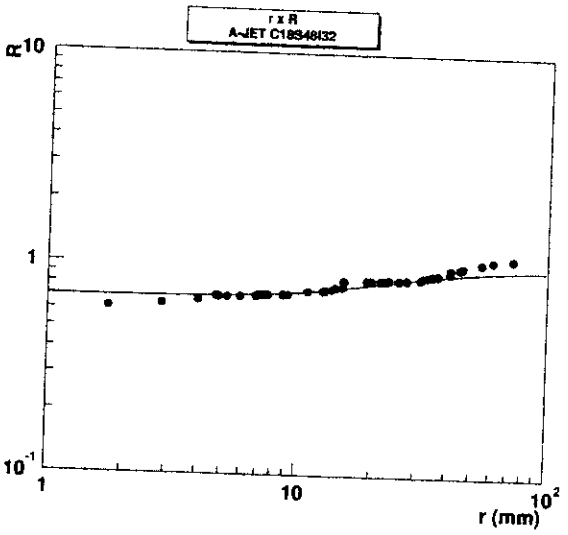

Fig. 3. Example of algorithm R for A-jet

reasoning for the isotropic characteristic coming from DW-plot. It it defined as,

$$mDW = \frac{1}{4M\Gamma}[\Sigma E_i + \frac{4}{\pi}\Sigma E_i(\Gamma\theta_i) + \Sigma E_i(\Gamma\theta_i)^2 + \frac{4}{3\pi}\Sigma E_i(\Gamma\theta_i)^3] \qquad (4)$$

In figure 4 this algorithm was applied for various A-jets, C-jets and also for Centauro events with the height determined through kinematics of $\pi^0 \rightarrow \gamma + \gamma$ and triangulation method. In fact, with the general expression above, it is also possible to calculate moments of order higher than 3^{rd}. In principle, addition of these greater order moments to the algorithm mDW could smooth this curve. The difficult comes from the normalization factor of these moments, for instance the 4^{th} moment has a $\log(1+\Gamma^2\theta^2)$ factor that does not converge at $\Gamma\theta \rightarrow \infty$.

3 Results and discussions

As 87 analysed events comes from a localized target of Carbon we have the vertex of the interaction point with the precision of the geometric distance of the gap, i.e. around 14% because the height is H=(170 ± 23)cm. This is not the case of A-jets. Then, for the events with difficult height determination, mainly A-jets, we used the algoritms in function of $r/\bar{r}$.

Defining 'sphericity' as the slope of best fitted mDW algorithm we got the histogram of this quantity in figure 5. Expected value of 2 for a isotropic decay of secondaries is not observed. Mean value of ad-hoc defined 'sphericity' is between 1.3 and 1.6, as got from the histogram, that means most of events are jet-like with A-jets more isotropical in zenital angle distribution. Improvement for these 'sphericity'values could be done, fitting the analytical curve in the

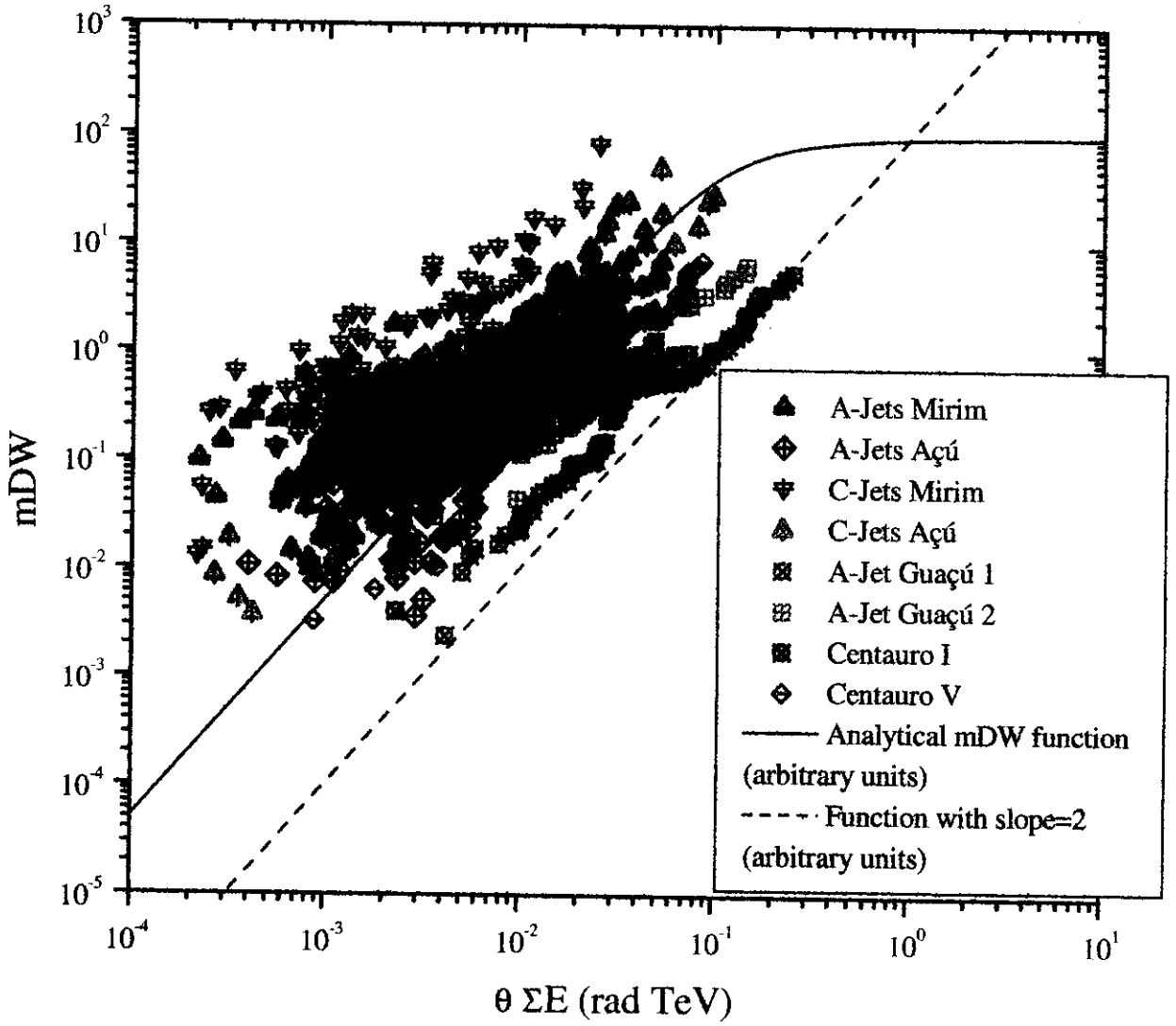

Fig. 4. Algorithm mdW for some events with measured interaction point

experimental data.
Also an application to 9,360 simulated events using CORSIKA/QGSJET procedure (Part of the results gotten, under this procedure and a simulation of emulsion chamber done by M.Tamada, were used in the reference, Tamada & Ohsawa (2000)) was done and used in a paper submitted to this conference (Search of centauro like events. C.R.A.Augusto et al. (2001)). The procedure is based on the CORSIKA5.20 code (Knapp et al. (1997)) where it is incoporated the QGSJET model (Kalmykov et al. (1994)).

Acknowledgements. We have pleasure in acknowledging our indebtetness to the financial support from CNEN, CNPQ, FAPESP, FINEP, UFF, UNICAMP in Brazil and Aoyama Gakuin University, University of Tokyo, Waseda University, Ministry of Education in Japan. We are also glad to IIF-UMSA in Bolivia, host of the experiments, for the help in many occasions. The authors wish to acknowledge to all members of B-J Collaboration for the free use of the data. One of us (EHS) is keen to express his gratitude to ICRR-University of Tokyo, where he was recipient of a COE fellowship.

Appendix A

Below, we list 6 moments obtained from a general expression in the text. For the purpose of this paper we used the first 4 moments, because the 5^{th} moment does not converge, in spite of the 6^{th} has a limit for $\Gamma\theta \to \infty$.

$$\Sigma E_i(\Gamma\theta_i)^0 \simeq M\Gamma[1 - \frac{1}{(1+\Gamma^2\theta^2)^2}] \quad \text{(A1)}$$

$$\Sigma E_i(\Gamma\theta_i)^1 \simeq M\Gamma[\frac{\arctan\Gamma\theta}{2} - \frac{(\Gamma\theta - \Gamma^3\theta^3)}{2(1+\Gamma^2\theta^2)^2}] \quad \text{(A2)}$$

$$\Sigma E_i(\Gamma\theta_i)^2 \simeq M\Gamma[\frac{\Gamma^2\theta^2}{1+\Gamma^2\theta^2}]^2 \quad \text{(A3)}$$

$$\Sigma E_i(\Gamma\theta_i)^3 \simeq M\Gamma[\frac{3\arctan\Gamma\theta}{2} - \frac{3\Gamma\theta + 5\Gamma^3\theta^3}{2(1+\Gamma^2\theta^2)^2}] \quad \text{(A4)}$$

$$\Sigma E_i(\Gamma\theta_i)^4 \simeq M\Gamma[2\log(1+\Gamma^2\theta^2)^2 - \frac{3\Gamma^4\theta^4 + 2\Gamma^2\theta^2}{(1+\Gamma^2\theta^2)^2}] \quad \text{(A5)}$$

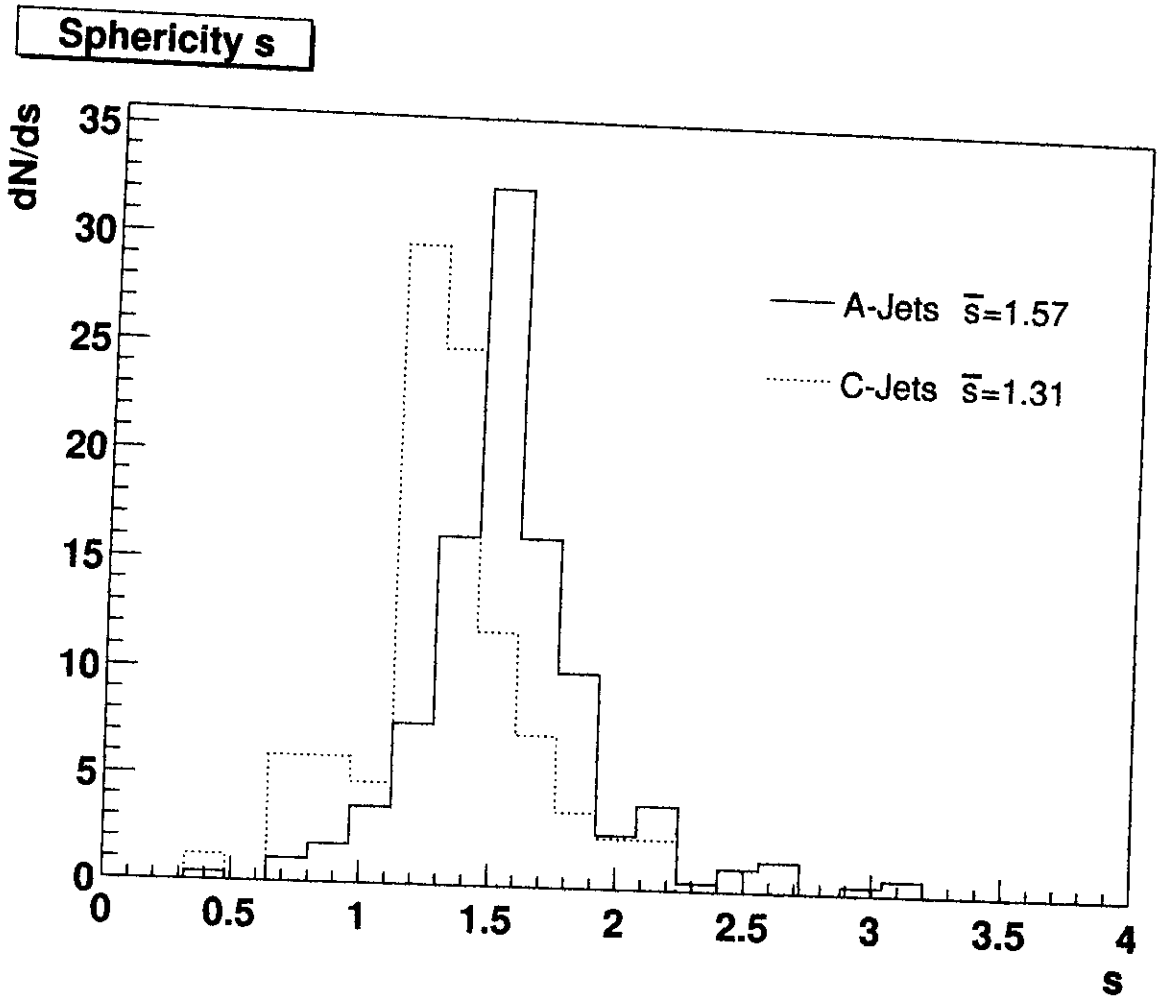

Fig. 5. Distribution of 'sphericity

$$\Sigma E_i(\Gamma\theta_i)^5 \simeq M\Gamma[\frac{3\Gamma^4\theta^4 - 4\Gamma^3\theta^3 + 18\Gamma^2\theta^2 + 4\Gamma\Theta + 3}{(1+\Gamma^2\theta^2)^2}] \times[\frac{\Gamma\Theta}{2} - \arctan\Gamma\theta] \quad \text{(A6)}$$

References

N.M.Duller and W.D.Walker, Phys.Rev.93,No.1,(1954),215.

Brasil-Japan Collaboration of Chacaltaya Emulsion Chamber Experiment, Prog.Theo.Phys.,Supp.76,(1983),1.

Shibuya,E.H., Proc. $XVIII^{th}$ ICRC,vol.11,(1983),97.

M.Tamada & A.Ohsawa, Nucl.Phys.B581,(2000),73.

C.R.A.Augusto et.al., accepted to be presented to this conference.

J.Knapp, D.Heck and G.Shatz, Nucl.Phys.B(Proc.Suppl.)52B (1997),136 & 139; D.Heck, J.Knapp, J.N.Capdevielle, G.Schatz & T.Thouw, Forschungszentrum Karlsruhe FZKA 6019(1998). Kernforschungszentrum

N.N.Kalmykov, S.S.Ostapchenko & A.I.Pavlov: Bull.Russ. Acad.Sci., Phys.Ser.58 (1994) 21; N.N.Kalmykov, S.S.Ostapchenko, Phys.At.Nucl. 56 (3), (1993), 346.

Proceedings of ICRC 2001: 1 © Copernicus Gesellschaft 2001

ICRC 2001

SEARCH OF CENTAURO LIKE EVENTS

C.R.A.AUGUSTO[1], S.L.C.BARROSO[2], P.C.BEGGIO[3], A.O.CARVALHO[2], M.J.MENON[2], C.E.NAVIA[1], R.OLIVEIRA[2], and E.H.SHIBUYA (BRAZIL-JAPAN COLLABORATION OF CHACALTAYA EMULSION CHAMBER EXPERIMENT)[2]

[1]Instituto de Física, Universidade Federal Fluminense, 24210-130 Niterói, RJ, Brazil
[2]Instituto de Física 'Gleb Wataghin', Universidade Estadual de Campinas, 13083-970 Campinas, SP, Brazil
[3]Laboratório de Ciências Matemáticas, Universidade Estadual do Norte Fluminense, Campos dos Goytacazes, RJ, Brazil

Abstract. Since 1971, Brazil-Japan Chacaltaya Emulsion Chamber Experiment is observing unusual events interpreted as Multiple Hadron Production without π^0 events. As previously reported, these events are characterized by high hadron content and no π^0 production at the interaction. Two of the five Centauro events have their interaction point determined through microscope measurements in the films of the emulsion chamber exposed at Mount Chacaltaya (5,220 m of altitude). In spite of the fact that exists other Centauro candidates, in this paper we present analysis on the beforehand mentioned 5 events because all have showers observed at both upper and lower chamber exposed at Chacaltaya and the total showers energy in the range (200-300)TeV. The comparison was done with 285 events through acceptance analysis of similar to the 5 selected Centauro events, using their physical quantities like: total energy ($\Sigma E_{showers}$), multiplicity ($n_{showers}$), emission angle related quantity ($r_{showers}$) and so on. It results that only 3 other events are comparable with Centauro events but neither of them has high hadron content. Sideways we compared with 9,360 computer simulated events and the result is only 1 compatible, in terms of the same used observables, with the 5 Centauro events.

1 Introduction

Brazil-Japan Collaboration on Emulsion Chamber Experiment (B-J Collaboration) observed unusual events with high percentage of hadrons in comparison with γ's. They are nicknamed Centauro events due to different aspects between upper and lower parts of the detector. Normal events have more showers in upper but this is not the case of the event Centauro I found in 1971. Other events with high content of hadrons were observed so far but neither of them has this remarkable characteristics. However others events have characteristics that justifies the classification as exotic events. In Table I it is written their characteristics and some of the events have other stricking features as presented below.

Correspondence to: E.H.Shibuya(shibuya@ifi.unicamp.br)

Centauro number	$\Sigma E_\gamma + \Sigma E_h^{(\gamma)}$ (TeV)	$n_\gamma + n_h$	*Height* (m)	*Remarks*
I	$9.0 + 221.5$	$1 + 49$	50^*	*most reliable*
II	$24.4 + 179.0$	$5 + 32$	80	*block corner*
III	$101.3 + 168.5$	$26 + 37$	230	*two blocks*
IV	$139.3 + 147.7$	$68 + 39$	500	*without central core*
V	$79.4 + 270.6$	$25 + 40^{**}$	500^*	*'Leading particle'*

Table 1. Main characterists of 5 Centauro events. The marks (*) indicates events with height determined directly, whereas the mark (**) corresponds to the highest energy hadron

2 Experimental description

A series of detectors named Emulsion Chambers have been exposed to Cosmic Radiation incident at mountain altitudes by B-J Collaboration, since 1962. This paper concerns to the observation of the secondaries produced by Hadronic Interactions induced by Cosmic Ray Particles incident on Mt.Chacaltaya (5220m above sea level and 20 km far from La Paz City, Bolivia). This Cosmic Rays Observatory (geomagnetic coordinates $4^0 50' 40''$ South and $0^0 50' 20''$ East) was inaugurated in scientific activities in the year 1947 with the π-μ events and since then are showing some remarkable scientific informations, maybe due to its privileged location in a direction of the center of Galaxy. Since 1969 the Emulsion Chambers settled there have area size comparable to the summed area of previous 13 previous detectors. Also an improvement of the experiments was the inclusion of a fixed target of asphalt pitch, nowadays blocks of compacted and amalgamated plastic sheets. Between the target and the floor of the room there is an air gap of 170 cm thick. Over the tar-

get and also over the floor are settled envelopes with photosensitive material inside them, constituting a kind of carpet. Inserted between the envelopes, there are lead plates working as a converter of electromagnetic particles in the electron/positron showers. The lead plates that are the converter would act also as a target material for hadronic particles. So, the photosensitive material (X-ray films and Nuclear Emulsion plates) registers showers of electron/positron converted from γ's coming mainly from π^0 decay. Other hadrons ($\pi^{\pm}$, p, n, etc.) could interact with the atmosphere molecules, carbon and lead, then obviously named A-jet, C-jets and Pb-jet, respectively. So, the spots seen in the films are always from γ's showers, these produced mainly by π^0's. By obvious reasons the upper and lower parts of the detector are called Upper and Lower Chamber. The event named Centauro I is unusual because it mimics an event coming from the botton and leaving to the atmosphere above the detector. That is not the case, because the measurements of shower spots results in an increasing distance between pairs of them as we go downstream inside the detector. So, the simplest and naive interpretation is to assume a Multiple Production of Hadrons without π^0's, as this behaviour is not usual for γ's. Since this event observation, other events with high content of hadrons were found. In spite of their similitude with the first one in this aspect, they present more showers in Upper than in Lower Chamber, as usually. An exception is the event named Centauro VIII which has recocgnizable showers only in the Lower Chamber. Besides the absence of signal in the upper part of the detector, this event has total energy very different from the selected Centauro candidates and by these reasons it was not included in the present analysis. Another remarkable Centauro event presenting stricking features is Centauro V(C16S086I037). This event has a peculiar characteristic of a very high energy shower (around 20% of total energy of showers) and 2 successive interactions in the Lower Chamber, without observable signal in the Upper Chamber. Moreover this Centauro candidate has a direct estimation of height ($500\ ^{+206}_{-113}$ m), through measurement on a distance of one pair of showers in both, Upper and Lower Chambers. Detailed analysis of Centauro V will be presented in (Improved analysis of one centauro candidate event. C.R.A.Augusto et al. (2001)).

3 Acceptance analysis

Measurements of $e^{\pm}$ in both X-ray films and/or Nuclear Emulsion plates, yields energy and multiplicity of showers, directly. Then, to look for Centauro similar events, we first did unsuccessful search for usual events with same parameters of Centauro ones.

From the informations on energy and multiplicity we estimate the energy weigthed center. So, all the following physical quantities (azimuthal and zenital angles, transverse momentum, etc.) depends on the energy. Even the multiplicity, that is one observable quantity, depends on the energy, through threshold energy effect. So, the next procedure to look for Centauro similar events was the total energy, using the Kolmogorov-Smirnov statistical analysis (Numerical Recipes in Fortran. W.H.Press et al. (1992)). The results are seen in figure 1, with separate plots for experimental events (87 C-Jets and 288 A-jets, including 5 Centauro events) and 9,360 simulated A-jets events (M.Tamada used CORSIKA/QGSJET and a simulation of the detector.Part of the results gotten, was used in the reference M.Tamada & A.Ohsawa (2000)) under CORSIKA5.20 code (Knapp et al. (1997)), employing QGSJET model (Kalmykov et al. (1994)). It is clear that both experimental events distributions looks similar, but they differ from simulated ones. Due to this and to the difference between experimental and uniform distribution, our conclusion is that the experimental distribution already is showing various types of interactions. Unfortunatelly, this analysis could not inform how much and which usual events are similar to the 5 Centauro ones.

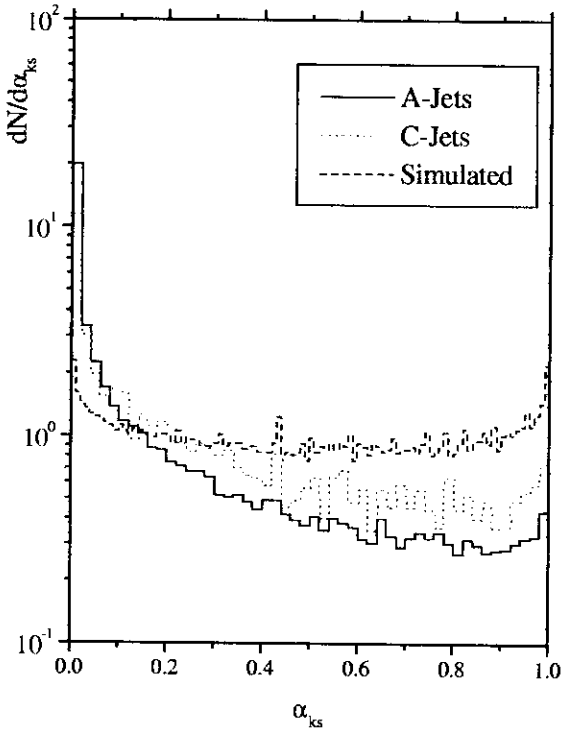

Fig. 1. Kolmogorov Smirnov parameter of pairs of events

Following the acceptance criteria we used other physical quantities (total energy, multiplicity, mean zenital angle, mean transverse momentum, azimutal angle, 'sphericity') and ad hoc statistical quantities ('dqm' and 'relm'). The quantity 'relm' is defined as a relationship between quantity of showers emitted forward, compared with the total multiplicity. We adopted for 'relm' ≥ 0.5. The quantity 'dqm' is defined as,

$$dqm = \frac{\sum_{i=1}^{N} \left(R_i - R(\bar{r}, r_i)\right)^2}{N} \qquad (1)$$

where N is the multiplicity and R is defined in the reference

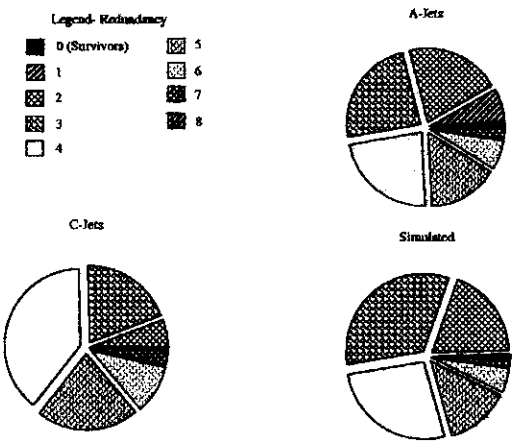

Fig. 2. Plots of 'surviving' events

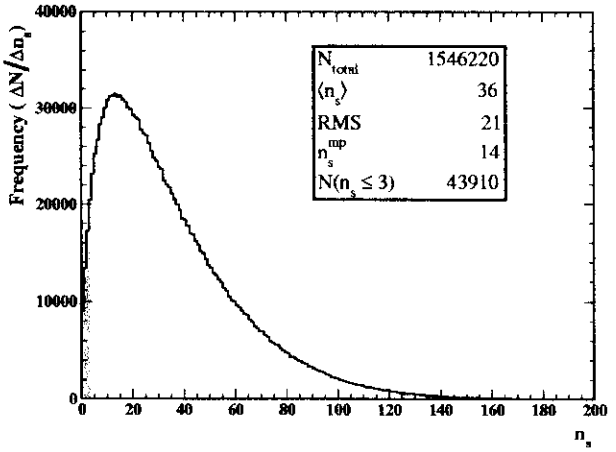

Fig. 3. 'Confidence' analysis

(Algorithms based on isotropic azimuthal angle distribution of interaction secondaries. C.R.A.Augusto et al. (2001)). There it is shown that the algorithm R is a function of Lorentz factor and zenital angle. When it is not possible to know the height of the interaction we could use a quantity proporcional to the zenital angle. In particular the algorithm R is convenient due to the opposite effects of height in both, Lorentz factor and zenital angle.

In this reference also there is the definition of 'sphericity'. As this quantity is obtained from an algorithm named mDW, the same favourable condition, mentioned above, is used to their estimation. These criteria are used to establish the acceptable range of the quantities of 5 Centauro events. Throwing out the usual events that are out of the ranges, we constructed a 'redundancy' figures, condensated in the figure 2. To each slice corresponds a number of criteria (see legend). The size of a slice is proportional to the number of families rejected by the correspondent number of criteria. The idea is to show that the major part of 'non-surviving' events are rejected by two or more criteria.

In the figure 3 it is presented an analysis about the independency of the results with the particular choice of 5 events. It is observed that in the sub-sample of 1.5×10^6 combination of any 5 events, the probability of getting 3 'survivors' is small ($\sim 3\%$).

4 Conclusions and discussions

Figure 4 presents results of C-jets and Centauro events of B-J Collaboration compared with acelerator data (Transverse momentum spectra for charged particles at the Cern Proton-Antiproton Collider.UA1 Collaboration (1992)) and (Multiplicity Dependence of the Transverse-Momentum Spectrum for Centrally Produced Hadrons in Antiproton-Proton Collisions at $\sqrt{s}$ = 1.8 TeV. T.Alexopoulos et al. (1988)). It is necessary to say that the C-jets data is for γ's and so, its P_T value must be multiplied by 2, approximately. This figure shows that Centauro events secondary particles, supposing as γ's, fits with C-jets events. However, from figure 2 we did not found any C-jet compatible with Centauro events. Then, only the Centauro secondaries, properly identified as hadrons, must be corrected by a factor of inclasticity, because in C-jets there are not predominancy of hadrons. Here, we used its mean value, $\bar{k}_\gamma = 0.3$ and the Centauro events occupaies a region of (0.8 - 1.8) GeV/c and (10 - 17) for mean transverse momentum and rapidity density, respectively. Even using $\bar{k}_\gamma = 0.4$, the mean transverse momentum region decreases to (0.6 - 1.4), somehow greater than acelerator data.

Acknowledgements. We have pleasure in acknowledging our indebtetness to the financial support from CNEN, CNPQ, FAPESP, FINEP, UFF, UNICAMP in Brazil and Aoyama Gakuin University, University of Tokyo, Waseda University, Ministry of Education in Japan. We are also glad to IIF-UMSA in Bolivia, host of the experiments, for the help in many occasions. The authors wish to acknowledge to all members of B-J Collaboration for the free use of the data. One of us (EHS) is keen to express his gratitude to ICRR-University of Tokyo, where he was recipient of a COE fellowship.

References

C.R.A.Augusto et al., accepted to be presented to this conference.
W.H.Press, S.A.Teukolsky, W.T.Vetterling, B.P.Flannery, Cambridge University Press, 1992.
M.Tamada & A.Ohsawa, Nucl.Phys.B581,(2000),73.
J.Knapp, D.Heck and G.Shatz, Nucl.Phys.B(Proc.Suppl.)52B (1997),136 & 139; D.Heck, J.Knapp, J.N.Capdevielle, G.Schatz & T.Thouw, Forschungszentrum Karlsruhe FZKA 6019(1998).
N.N.Kalmykov, S.S.Ostapchenko & A.I.Pavlov: Bull.Russ. Acad.Sci., Phys.Ser.58 (1994) 21; N.N.Kalmykov, S.S.Ostapchenko, Phys.At.Nucl. 56 (3), (1993), 346.
C.R.A.Augusto et al., accepted to be presented to this conference.
G.Arnison et al., Phys.Lett.118B,(1982),167.
T.Alexopoulos et al., Phys.Rev.Lett.60,No.16,(1988),1622.

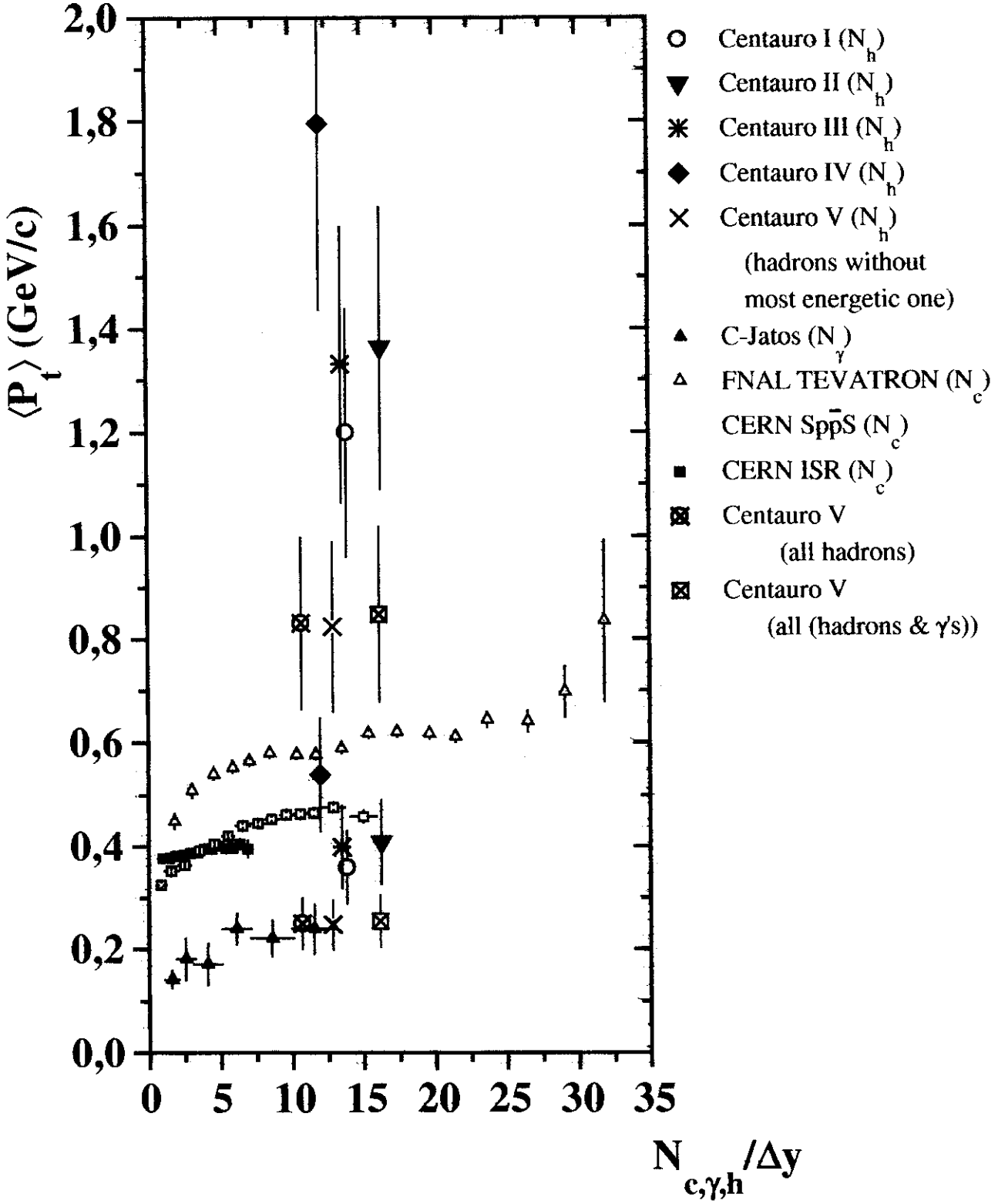

Fig. 4. P_T - rapidity density correlation

Proceedings of ICRC 2001: 1 © Copernicus Gesellschaft 2001

ICRC 2001

IMPROVED ANALYSIS OF ONE CENTAURO CANDIDATE EVENT

C.R.A.AUGUSTO[1], S.L.C.BARROSO[2], P.C.BEGGIO[3], A.O.CARVALHO[2], M.J.MENON[2], C.E.NAVIA[1], R.OLIVEIRA[2], and E.H.SHIBUYA (BRAZIL-JAPAN COLLABORATION OF CHACALTAYA EMULSION CHAMBER EXPERIMENT)[2]

[1]Instituto de Física, Universidade Federal Fluminense, 24210-130 Niterói, RJ, Brazil
[2]Instituto de Física 'Gleb Wataghin', Universidade Estadual de Campinas, 13083-970 Campinas, SP, Brazil
[3]Laboratório de Ciências Matemáticas, Universidade Estadual do Norte Fluminense, Campos dos Goytacazes, RJ, Brazil

Abstract. In a series of experiments of emulsion chambers exposed at Mt. Chacaltaya a remarkable event with high content of hadrons was observed. Moreover, this event has a hadron that interacts twice at deeper layers of the detector and that has energy between (16-20)% of the total energy of main interaction, the former figure for all particles and the last only for hadrons. Due to these facts it was interpreted as a surviving hadronic particle and its transverse momentum results between ($460/k_\gamma$ and $680/k_\gamma$)MeV/c. The last is obtained considering the center of only 40 particles identified as hadrons while the first one is obtained with all 60 particles, irrespectively of their identification as γ or hadron. Other results, mainly concerned with a γ-hadron identification will be presented, showing the reasons to classify this event as a Centauro type.

1 Introduction

The so-called Centauro events were first observed by Brazil-Japan Collaboration on Emulsion Chamber Experiment (B-J Collaboration), exposed during the period 1969-1970. Following this exposure a chamber denominated chamber no.16 was exposed in the period 1971-1972 and there was observed a second good example of Centauro candidate. This chamber is very thick in a lower part of the detector, till 30 r.l. and contains 2 X-ray films each 2 r.l., besides 10 Nuclear Emulsion plates. The upper part has 12 r.l., 2 X-ray films also inserted each 2 r.l. and 3 Nuclear Emulsion plates. Therefore the chamber is a good detector for hadrons recognition. The misfortune is that some Emulsion plates were dammaged by fading and the measurements was postponed for a couple of years. Concerning to the event observed in the upper chamber block S086, continuing to lower chamber block 1037, the quality of 64 X-ray films and 13 Emulsion plates are quite good, with few exceptions. This event measurement was postponed to around 1979, by the reasons above mentioned and also due to the fact that the upper block is at Campinas and the lower block was at Rio's lab.

As was presented in many occasions, the Centauro events are naively interpreted as multiple production of hadrons without π^0's. The interpretation was caused by the first Centauro analysis, due to the high content of hadrons compared with γ's, those produced mainly through π^0 decay. After Centauro I we looked for hadron rich events and so, Centauro events recognition is strongly dependent of hadron-γ's discrimination.

Then, careful and detailed re-measurements were done, by different scanners and improved devices. In paralel, improvements in the energy determination, analysis methods, etc. was carried out and reported at various conferences.

The main purpose of this paper is to present the last results on the Centauro V (C16S0861037), aiming to increase confidence on hadron identification. Together with the analysis to be reported in ((Search of Centauro like events. C.R.A.Augusto et al., 2001)) we complete the reasoning to justify the conclusions, there presented, mainly on the mean transverse momenta and rapidity density ($< P_T >$ - $N_{c,\gamma,h}/\Delta Y$) correlation, that shows a different figures for Centauro events compared with usual cosmic ray and acelerators events.

2 Hadron identification

It is a very difficult task in Emulsion Chamber experiments to identify a single ionizing track, because it traverses only the thickness (50 μm) of sensitive material. Moreover, many ionizing tracks, as background, are detected by Emulsion plates, difficulting single track recognition. The way to identify ionizing tracks is to look for groups of tracks (at least 100 paralel tracks in an area of $50^2 \mu m^2$) constituing showers of eletromagnetic particles. Then, a straightforward identification of hadrons is possible using some criteria for that purpose.

The most reliable one is through the behaviour of showers inside the chamber, i.e., usual γ induced showers have not two or more maxima in the transition curve. Another confi-

Correspondence to: E.H.Shibuya(shibuya@ifi.unicamp.br)

dent criterion is on probability arguments for showers starting deep in the detector, as the probability is $\sim \exp(-t)$, with t, measured in r.l., means the depth where the shower starts to be observed. We used t = 9 r.l. in the analysis of the event C16S086I037.

As this chamber have many Emulsion plates, the visual recognition of groups of showers separated at least by a distance of 20 μm is an additional criterion for hadron identification. So, the combination of these criteria with a best fitting, through computer software especially written for types of blocks used by B-J Collaboration, yields this improved analysis of the event described in the paper. For instance, shower #27 is observed in upper chamber and penetrates through lower chamber and clearly its fitting for only one transition curve is unreasonable. Besides, the observation of Emulsion plates shows 5 showers in the upper part and 3 in the lower. Separate transition curve are shown in Figures 1 and 2. To have the total transition of this shower, it is necessary to shift the horizontal axis of lower block plot by 0.59 r.l., shift that corresponds to the sum of air gap and asphalt pitch layers.

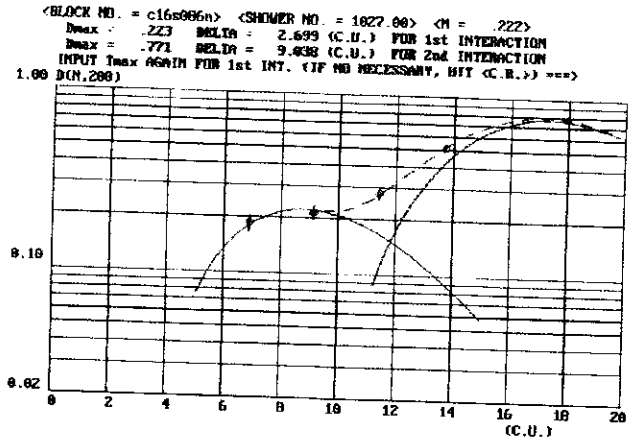

Fig. 1. Transition curve in upper block 086

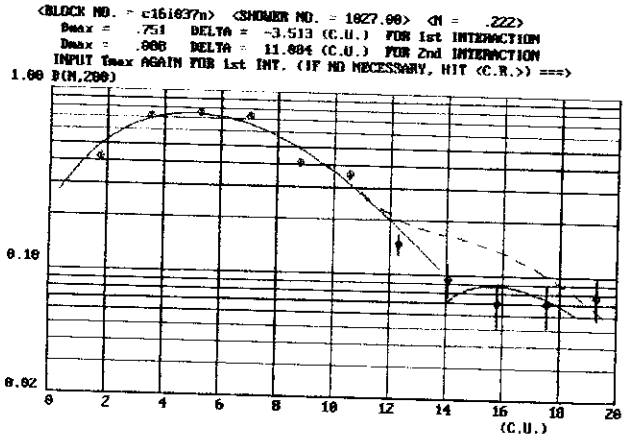

Shower #62 is interpreted as a surviving particle. At the same time it carries 20% of the total energy of identified hadrons and so, it is also a leading particle. It is surviving because it has not observable signal in the upper part of the chamber and it presents two maximum only in lower chamber, as a Figure 3 shows.

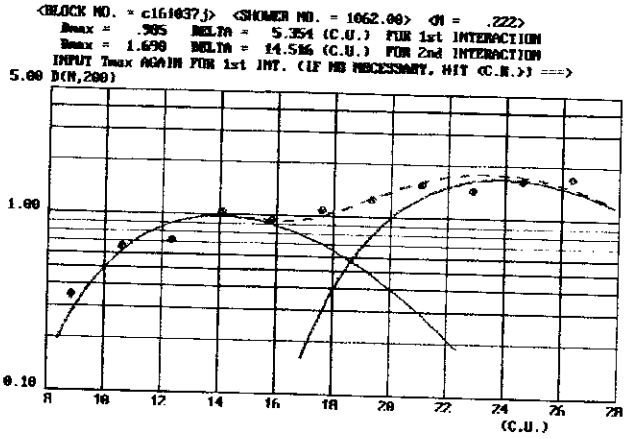

Fig. 3. Shower #62, interpreted as surviving and leading particle

3 Discussions

Zenital angle corrected map is presented in Figure 4 and condensed results are in the following Figure 5.

It is necessary to say that the we adopted a rather severe procedure, i.e. we classified as hadrons only if the shower obeys at least one criterion. This situation was relaxed for 3 showers classified in a H6 class, but in the other hand another 3 showers classified as G2 class, that is as γ's, seems hadronic originated ones. In fact doing a starting point integral distribution the best fit shows that also all 20 γ could be interpreted as hadronic origin particles and that decaied during its propagation in the atmosphere.

Acknowledgements. We have pleasure in acknowledging our indebtetness to the financial support from CNEN, CNPQ, FAPESP, FINEP, UFF, UNICAMP in Brazil and Aoyama Gakuin University, University of Tokyo, Waseda University, Ministry of Education in Japan. We are also glad to IIF-UMSA in Bolivia, host of the experiments, for the help in many occasions. The authors wish to acknowledge to all members of B-J Collaboration for the free use of the data. One of us (EHS) is keen to express his gratitude to ICRR-University of Tokyo, where he was recipient of a COE fellowship.

References

C.R.A.Augusto et al., accepted to be presented to this conference.

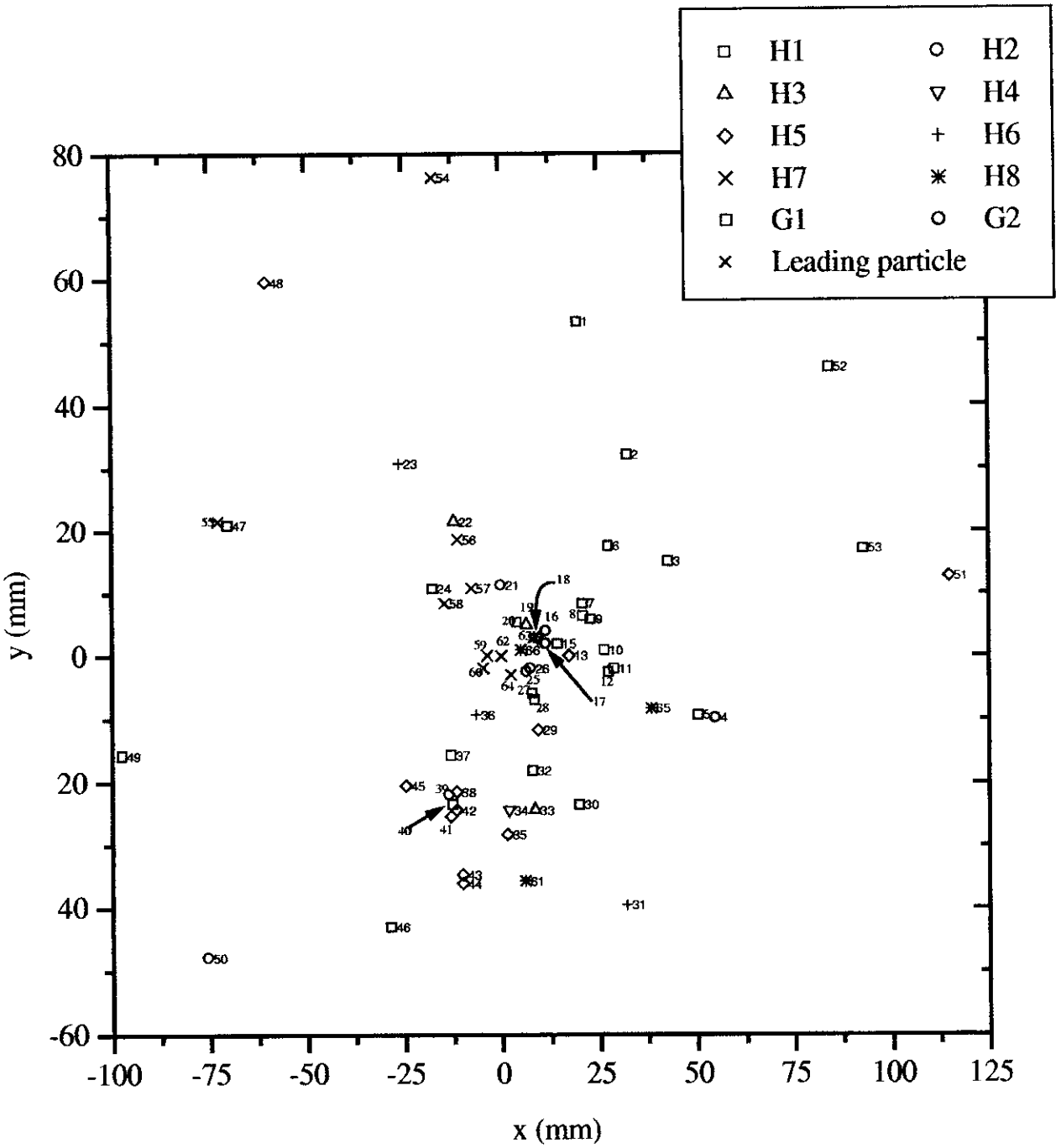

Fig. 4. Upper and Lower blocks superposed map

Centauro V (C16S086I037)

Classification of γ's

Upper Chamber		Lower Chamber	Total
G1	G2		
17	3	0	20

G1: fitted one curve in X-ray films
#: 1, 2, 3, 5, 6, 7, 9, 12, 15, 24, 30, 32, 46, 47, 49, 52 and 53
G2: two cores observed in Emulsion plate
#: 4, 16 and 17

Classification of hádrons

Upper						Lower		Total
H1	H2	H3	H4	H5	H6	H7	H8	
7	4	3	2	9	3	9*	4	41*

H1: it starts in upper, penetrates through lower and has multi-cores (at least 2 at upper and/or lower). #20 and #27 was used for height determination in both, X-ray films and Emulsion plate.
#: 8(1 up. and 2 lo.), 10(2 up. and 2 lo.), 11(2 up. and 1 lo.), 20(4 up. and 2 lo.), 27(5 up. and 3 lo.)+28(fits more than one curve), 37(2 up. and 1 lo.) and 40(4 up. and 2 lo.)
H2: no. of cores ≥ 3 (≡ A-jets).
#: 21(4 cores), 25(4 cores and fits with more than one curve)+26, 39(3 cores) and 50(3 cores and fits with more than one curve)
H3: no. of cores = 2 (≡ A-jets) and fits with more than one curve.
#: 19, 22 and 33
H4: it appears at ~9 c.u. and fits with more than one curve
#:18(1 core at 12 c.u.) and 34(2 cores at 12 c.u.)
H5: fits with more than one curve
#: 13, 29, 35, 41, 38+42, 43+44, 45, 48 and 51
H6: it seems that fits with more than one curve
#: 23, 31 and 36

H7: no single transition curve, shows multi-cores (≡ C-jets) and penetrates till 22 c.u. #62* was identified as 'surviving particle' because it is absent in upper chamber, penetrates from 6 c.u. till 30 c.u. in lower chamber where shows at least two curves and contents ~18% of total observed energy
#: 54, 55, 56, 57, 58, 59, 60, 62* and 64
H8: no single transition curve, observed only after ~6 c.u. till ~24 c.u. (≡ Pb-jets)
#: 61, 63(till 22 c.u.), 65(after 4 c.u.) and 66(after 4 c.u.)

Fig. 5. Table of all showers measured in the event

Proceedings of ICRC 2001: 1 © Copernicus Gesellschaft 2001

ICRC 2001

Penetrating cascade showers observed by the emulsion chamber at high mountains

M.Tamada

Faculty of Science and Engineering, Kinki University, Osaka 577-8502, Japan

Abstract. The penetrating characteristics of the cascade showers observed by emulsion chambers at high mountains are studied by comparing with those in the simulated events obtained by the full Monte Carlo calculations through the atmosphere and the detector. A study is made for the Chacaltaya two-storey chambers and also to the Pamir joint carbon chambers applying just the same procedure both in the experiments and simulations. Although each chamber has a different structure, we find, in both chambers, an excess of the number of penetrating showers over the expectations. It amounts to $\sim 26\%$ of the penetrating showers in the Chacaltaya chambers and $\sim 43\%$ in the Pamir joint chambers.

1 Introduction

The Chacaltaya and Pamir emulsion chamber experiments have shown that there exist unusual phenomena which are not yet observed in the present accelerator experiments from the detailed analysis of high energy cosmic-ray families (a bundle of electromagnetic particles and hadrons produced in the nuclear and electromagnetic cascade process in the atmosphere) (Baradzei et al., 1992). Those are called 'Centauro-species', multiple hadron production without association of π^0-mesons. It is also discussed that the nature of secondary particles is possibly different from that of ordinary hadrons in those unusual phenomena based on the frequent observation of strong penetrating showers which became rejuvenated after passing through the target layer. In the paper (Funayama and Tamada,1984; Tamada,2001) we discussed about unusual behaviour of cascade development of the high energy showers in high-energy cosmic-ray families observed by Chacaltaya two-storey chambers no.18 and no.19. We studied in detail how the shape of the transition curve on the spot darkness of the observed showers, which penetrate from the upper chamber down to the lower chamber, deviate from that of (e,γ)-induced showers and of hadron-induced ones, and how often we can observe such penetrating showers, comparing experimental data with simulated cascade showers induced by (e,γ)-particles and by local hadron-interaction in the chamber assuming proper energy spectrum and zenith angle distribution. In the experiment, we can study such penetrating nature using the showers observed in the events which have at least two penetrating showers, because an exact upper-lower correspondence is necessary to do the analysis and is possible only for those events. It is, however, not easy to estimate how the above selection of the events distort the average characteristics of the families and of penetrating showers. Here we perform full Monte-Carlo calculation of the atmospheric families throughout the atmosphere and the detector, and apply just the same procedure both to the experimental and simulational data in order to make possible a direct comparison between the two.

Correspondence to: M.Tamada (tamada@me2.kindai.ac.jp)

2 The structure of the two-storey chambers

Fig.1 shows the basic structure of the Chacaltaya two-storey chambers no.18 and no.19 and of Pamir joint chamber P3'. The Chacaltaya chamber no.19 (no.18) consists of the upper chamber of 6 (7) cmPb, the target layer of 23 cm carbon (petroleum pitch), wooden support of 5cm thick, the air gap of 158 cm height and the lower chamber of 8.4 (9.6) cmPb. Four (five) sensitive layers (N-type X-ray film and nuclear emulsion plate) are inserted in the upper chamber and eight (nine) sensitive layers in the lower chamber. The Pamir joint carbon chamber P3' consists of the upper chamber of 6cm Pb, the target layer of 60 cm carbon and the lower chamber of 5 cmPb. The sensitive layers (N-type X-ray films) are inserted under 4 and 6 cmPb in the upper chamber and under 3 and 5 cmPb in the lower chamber. The shower, a bundle of electrons, induced by (e,γ)-particles or hadron interaction in the chamber, produce a small dark spot on the developed X-ray films at several successive layers. These shower spots are visible by the naked-eyes. The darkness detection threshold of the shower spot, measured by a $200 \times 200\mu m^2$ slit, is

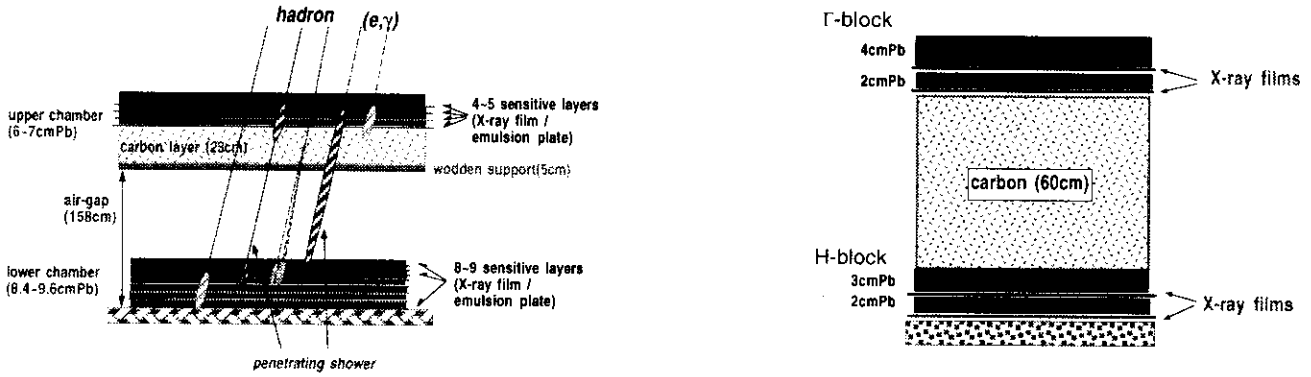

Fig. 1. Illustration of Chacaltaya two-storey chambers (left) and of Pamir joint chamber P3' (right).

around $D = 0.1$ for the N-type films.

3 Simulations of the atmospheric families

We use CORSIKA/QGSJET simulation code (Heck et al., 1998) for generating atmospheric families. 20,000 primaries of $E_0 \geq 10^{15}$ eV for the Chacaltaya chambers and 40,000 primaries for the Pamir chambers are sampled from the energy spectrum of 'normal chemical composition'. Nuclear and electromagnetic cascade in the atmosphere are followed until the energy of all the produced particles fall below 1 TeV or they arrive at the observation level. Zenith angle of the primary particles is selected at random in the interval between $0°$ and $45°$.

4 Detector simulation

For (e, γ)-particles and hadrons in the event, arriving upon the chamber, with total energy larger than 100 TeV, we calculate further nuclear and electromagnetic cascade development inside the chamber taking into account exactly the structure of each chamber.

4.1 Hadron-induced showers

We use QGSJET (Kalmykov et al.,1994) model for hadron-nucleus interactions, which is based on the Gribov-Regge theory of multiple Pomeron exchanges. In the nuclear cascade all hadrons, produced in the collisions during passage through the chamber, are followed until their energy falls below 80 GeV or they leave the chamber. The interaction mean free path of hadron-nucleus interactions is assumed to decrease with increasing interaction energy, e.g., $\Lambda_{p-Pb} = 15.9$ cm, $\Lambda_{\pi-Pb} = 17.5$ cm, $\Lambda_{K-Pb} = 18.0$ cm, $\Lambda_{p-C} = 56.1$ cm, $\Lambda_{\pi-C} = 71.3$ cm and $\Lambda_{K-C} = 78.5$ cm at $E = 10^{14}$eV. [1]

[1]For the Pamir chambers we take $\Lambda_{p-C} = 71.9$ cm, $\Lambda_{\pi-C} = 91.3$ cm and $\Lambda_{K-C} = 100.5$ cm at $E = 10^{14}$eV assuming the density of carbon layer is 1.0.

Since the shower-spot formation is mainly determined by high energy $\gamma-$rays, we further calculate the three-dimensional electromagnetic cascade development in the chamber for γ-rays of $E_\gamma \geq 1$ GeV, which are mainly decay products of π^0's produced in the collisions, using the Monte-Carlo code formulated by Okamoto and Shibata (1987), in which the LPM effect is also taken into account. Electrons and photons are followed until their energies fall below 1 MeV. Simulating electromagnetic cascade initiated by all the γ-rays of $E_\gamma \geq 1$TeV, we obtain the lateral distribution of the electron number density under every lead plate for the whole depth of the chamber. The electron number density, ρ_e, is converted to the local spot darkness, d, of X-ray film, by using the characteristic relation for the N-type X-ray film, [2] and finally we obtain the transition curve of the spot darkness D, measured by a $200 \times 200 \mu$m^2 slit, *vs.* depth T throughout the chamber. The experimental error of the measurement of spot darkness D is also taken into account by adding noise ΔD in each spot darkness where ΔD is sampled from Gaussian distribution with $\sigma_D = 0.1D$.

4.2 (e, γ)-induced showers

We also calculate electromagnetic cascade development in the chamber initiated by γ-rays and electrons in the events arriving upon the chamber, using the above mentioned Monte-Carlo code of electromagnetic cascade.

We thus obtain spot darkness throughout the chamber for all the member showers ((e, γ)- and hadron-origin) in the family. The visible (detectable) energy of each shower is re-

[2]The sensitivity of X-ray films depends on the conditions of the exposure and development. Then it differs a little chamber by chamber. The calibration is carried out by track-counting method using accompanied nuclear emulsion plate. (In the Pamir joint chamber, we have several blocks, for the calibration, with sensitive layers composed of both X-ray films and nuclear emulsion plates.) Applying the calibration procedure in each chamber, it is found that the films have just a standard sensitivity in the chamber no.19, but they have 30 % more sensitivity in the chamber no.18 and 40 % less in the Pamir chamber P3'.

Table 1. Number of high energy showers in the atmospheric families of $100 \leq E_{tot} < 1,000$ TeV with more than two penetrating showers observed in the Chacaltaya chambers no.18, no.19 and Pamir chamber P3'.

	chamber no.18		chamber no.19		Pamir P3'	
	experiment	simulation	experiment	simulation	experiment	simulation
no. of events	10		12		49	
(a) showers observed only in the upper chamber (non-penetrating), $E(\gamma) \geq 10$TeV	42	38.4 ± 1.2 ($34.8\ e,\gamma$ / $3.6\ h$)	50	48.4 ± 1.5 ($44.0\ e,\gamma$ / $4.4\ h$)	232	238.3 ± 6.5 ($207.0\ e,\gamma$ / $31.3\ h$)
(b) showers observed only in the lower chamber, $E(\gamma) \geq 10$TeV	8	8.7 ± 0.5	7	7.3 ± 0.6	28	60.0 ± 3.2
(c) penetrating showers†	26	21.0 ± 0.9 ($11.9\ e,\gamma$ / $9.1\ h$)	41	28.3 ± 1.1 ($20.8\ e,\gamma$ / $7.5\ h$)	96	53.8 ± 3.1 ($41.4\ e,\gamma$ / $12.4\ h$)
(d) excess of penetrating showers over expectation	5 ± 5.2	12.7 ± 6.5 / 17.7 ± 8.3			42.2 ± 10.3	

Numerical values in the simulated events are normalized to the number of experimental events. Numerical values in the parenthesis are those of (e,γ)-induced and hadron-induced showers.
†) number of showers with $N_{upper}(D \geq 0.2) \geq 2$ and $N_{lower}(D \geq 0.2) \geq 1$ chosen irrespective of its energy.

estimated by applying fitting procedure. That is, from a set of standard transition curves of $D^{std}vs.T$, calculated for showers of electron-positron pair origin taking into account the exact chamber structure, the best fit is selected by choosing the energy value, E, and the first pair-creation depth, ΔT, by a computer algorithm employing the gradient descent method for a search of the chi-square minimum.

5 Selection of the events

For the Chacaltaya chambers we selects events for the analysis which satisfy the following conditions;
1) the total visible energy, E_{tot}, is in the interval between 100 TeV and 1,000 TeV where minimum shower energy is taken to be 2 TeV and
2) the event has at least two penetrating showers in which the spot darkness at the bottom two layers in the upper chamber is larger than $D \geq 0.2$ and that at two successive layers in the lower chamber is larger than $D \geq 0.1$.

For the Pamir joint chamber we put the selection condition as;
1) E_{tot} is in the interval between 100 TeV and 1,000 TeV where minimum showers energy is taken to be 4 TeV and
2) the event has at least two penetrating showers in which the spot darkness of three layers among four sensitive layers at the experimental position is larger than $D \geq 0.1$.

The second condition is necessary to confirm the exact upper-lower correspondence. We observe 26 and 18 events with $100 \leq E_{tot} < 1,000$ TeV in one half of the Chacaltaya chamber no.18 and of no.19 respectively. 10 ($\sim 40\%$) among 26 events and 12 (~ 65 %) among 18 events satisfy the second selection criterion. In the Pamir joint chamber P3', we observe 91 events with $100 \leq E_{tot} < 1,000$ TeV. 49 (~ 55 %) events among them satisfy the second criterion. We apply just the same selection criteria also to the simulated events.

6 Penetrating cascade showers

In the events selected by the above two criteria some of the showers observed in the upper chamber can be followed down into the lower chamber. The observed high-energy showers are then classified into the following three categories.
(a) showers with visible energy $E(\gamma) \geq 10$ TeV observed only in the upper chamber (*non-penetrating showers*) defined as those which have no shower-spots of $D \geq 0.2$ in the lower chamber,
(b) those observed only in the lower chamber (C-jets, Pb-jets-lower) defined as showers which have no shower spots of $D \geq 0.1$ in the upper chamber and
(c) *penetrating showers*, irrespective of its energy, *re-defined* as a shower in which the spot darkness, D, is larger than 0.2 at least in two layers in the upper chamber, $N_{upper}(D \geq 0.2) \geq 2$, and at least in one layer in the lower chamber, $N_{lower}(D \geq 0.2) \geq 1$. A typical example of the transition curve of the penetrating shower is shown in Fig.2.

We summarise in Table 1 the number of showers of the three categories in the above selected events.

In order to demonstrate how the selection criterion (2) distort the average characteristics of the atmospheric families, we show in Table 2 the number of showers of the above three categories ((a), (b) and (c)) for the simulated events which satisfy the condition (1), i.e., events with $100 \leq E_{tot} < 1,000$ TeV, and those for the events which satisfy both criteria (1) and (2) respectively. As is seen in the table, the second criterion works in favour of more penetrating showers, 1.6 $\sim$ 1.8 times more than the average of all the events.

Table 2. Number of high energy showers per event in the simulated events.

selection criteria	chamber no.18 (1) and (2) (290 events)	chamber no.18 (1) (611 events)	chamber no.19 (1) and (2) (269 events)	chamber no.19 (1) (470 events)	Pamir P3' (1) and (2) (277 events)	Pamir P3' (1) (528 events)
(a)	3.84 ± 0.12 ($3.487\ e,\gamma$ / $0.36\ h$)	3.05 ± 0.07 ($2.77\ e,\gamma$ / $0.28\ h$)	4.03 ± 0.12 ($3.66\ e,\gamma$ / $0.37\ h$)	3.42 ± 0.09 ($3.12\ e,\gamma$ / $0.30\ h$)	4.86 ± 0.13 ($4.22\ e,\gamma$ / $0.64\ h$)	3.56 ± 0.08 ($3.11\ e,\gamma$ / $0.454\ h$)
(b)	0.87 ± 0.05	0.76 ± 0.04	0.61 ± 0.05	0.60 ± 0.04	1.22 ± 0.07	1.14 ± 0.05
(c)	2.10 ± 0.09 ($1.18\ e,\gamma$ / $0.92\ h$)	1.21 ± 0.05 ($0.64\ e,\gamma$ / $0.57\ h$)	2.36 ± 0.09 ($1.73\ e,\gamma$ / $0.63\ h$)	1.49 ± 0.06 ($1.08\ e,\gamma$ / $0.41\ h$)	1.10 ± 0.06 ($0.84\ e,\gamma$ / $0.25\ h$)	0.72 ± 0.04 ($0.53\ e,\gamma$ / $0.19\ h$)

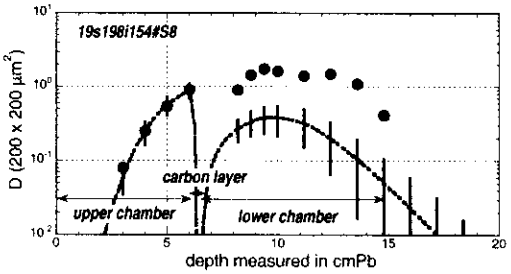

Fig. 2. An example of the transition curve on spot darkness of the penetrating showers observed in Chacaltaya chamber no.19. Dotted curve is an expected shower transition curve.

It is remarkable that the number of hadron-induced penetrating showers is almost same to that of showers in lower with $E(\gamma) \geq 10$ TeV in the Chacaltaya events. In Table 1 we show the number of showers of the three categories expected in the simulated events for the comparison with experimental data. Here the numerical values are normalized to the experimentally observed number of events in each chamber. We can see no considerable differences between simulations and experiments in the number of non-penetrating showers and showers in lower, except for the showers in lower in the Pamir chamber P3' where the simulational data gives ~ 2 times more than experimental value. For the penetrating showers, we can see around one half of the experimental penetrating showers can be explained by the (e,γ)-induced showers in all the three chambers. The other half of the penetrating showers then is expected to be hadron-induced ones, but it is seen that the number of those expected in the simulated events is much smaller than the observation, though the statistics is small in the Chacaltaya chambers. The raw (d) in the table gives the excess of the number of the penetrating showers over the expectation. It amounts to $\sim 26\%$ of the penetrating showers in the Chacaltaya chambers and $\sim 43\%$ in the Pamir joint chamber P3'.

7 Discussions

We have studied in detail the penetrating probability of showers in high energy atmospheric families observed by the Chacaltaya two-storey chambers and by the Pamir joint chambers. In order to make possible a direct comparison with experiment we carried out full Monte Carlo calculations of the atmospheric families throughout the atmosphere and the detector taking into account the exact structure of the chamber. The comparison shows that there exists a considerable excess of penetrating showers in the experiments over the expectation, accounting for ~ 26 % of all the penetrating showers in the Chacaltaya chambers and ~ 43 % in the Pamir joint chamber P3'. One of the possible explanations for the observed excess in the experiments is to assume the occurrence of extremely collimated pair of a γ-ray and a hadron. That is, if the mutual distance between a γ-ray and a hadron is extremely small, e.g., less than ~ 1 mm, and the γ-ray-induced shower is observed in the upper chamber and the hadron-induced shower is observed in the lower chamber, we would possibly misidentify those two as a penetrating shower. If a γ-ray makes electromagnetic interactions in the atmosphere, we can observe collimated several (e,γ)-particles and a hadron as a 'mini-cluster' which are often found in the exotic events (Baradzei et al.,1992). Possible existence of hadron-bundles in which the mutual distance of the constituent hadrons is extremely small is also discussed in the analysis of transition curve of high-energy hadronic showers observed in the Pamir thick lead chamber (Tamada and Kopenkin,1997; Tamada and Ohsawa,2000).

Acknowledgements. This work is supported by Faculty of Science and Engineering of Kinki University, grant RK13-23.

References

Baradzei,L.T. et al.(Chacaltaya and Pamir collaboration), *Nucl. Phys. B* **370** (1992) 365

Funayama,Y. and Tamada,M., *J. Phys. Soc. Japan* **55**, (1986) 2977

Heck,D. et al., *FZKA report 6019, Forschungszentrum, GmbH Karlsruhe* 1998

Kalmykov,N.N., Ostapchenko,S.S., & Pavlov, A.I., *Bull. Russ. Acad. Sci. (physics)* **58** (1994) 1966

Okamoto,M and Shibata,T., *Nucl. Instr. Meth.* **A257** (1987) 155

Tamada,M. and Kopenkin,V.V., *Nucl. Phys. B* **494** (1997) 3

Tamada,M. and Ohsawa,A., *Nucl. Phys. B* **581** (2000) 73

Tamada,M., *Nucl. Phys. (Proc. Suupl.)* 97 (2001) 150

Proceedings of ICRC 2001: 1 © Copernicus Gesellschaft 2001

ICRC 2001

Observation of cosmic ray hadron interactions with Pamir 60 cm lead X-ray emulsion chamber

Y. Fujimoto[1], V. Kopenkin[2,5], A. Ohsawa[2], M. Tamada[3], C.E. Navia[4], C.R.A. Augusto[4], A.K. Managadze[5], T.M. Roganova[5], I.V. Rakobolskaya[5], and L.G. Sveshnikova[5]

[1] Advanced Research Institute for Science and Engineering, Waseda University, 3-4-1, Okubo, Shinjuku-ku, Tokyo 169, Japan.
[2] Institute for Cosmic Ray Research, University of Tokyo, Kashiwa-no-ha 5-1-5, Kashiwa, Chiba 277-8582, Japan
[3] Faculty of Science and Engineering, Kinki University, Osaka, 577-8502, Japan
[4] Instituto de Fisica, Universidade Federal Fluminense, 24020-130 Niteroi, Rio de Janeiro, Brazil
[5] Skobeltsyn Institute of Nuclear Physics, Moscow State University, Moscow, 119899, Russia

Abstract. In present paper we analyze experimental data from collaboration work of MSU and Waseda University with 60 cm lead chambers of recent $57m^2$ year exposure at Pamirs. With new method of determination of energy and identification of origin of showers we study features of gamma hadron families, single hadrons and gamma showers. Our data are in agreement with previous results obtained by MSU group. General characteristics of cosmic ray hadron interactions at high energies are discussed.

1 Introduction

Experiments with emulsion chambers have been carried out for more than 30 years at Mt. Chacaltaya (5200 m, Brazil-Japan Collaboration), Pamir (4300 m, Pamir Collaboration), Mt. Fuji (3750 m, Fuji Collaboration), Mt. Kanbala (5500 m, China-Japan Collaboration). The main objective of these experiments is to study fragmentation region of hadron interactions and primary composition at energies $10^{15} - 10^{17}$ eV. This is overlapping region with current collider experiments.

Nuclear electromagnetic cascade originated by primary cosmic ray particle in the atmosphere is detected in the chamber in the form of bundle of gamma rays and hadrons called a family. The study of family characteristics is a main subject in experiments with emulsion chambers at mountain altitudes.

Our experimental data is a complete set of data obtained through investigation of total available experimental area of X-ray films of total exposure $ST = 57m^2year$ collected with Pb chambers during 1988-1991 at Pamir. X-ray films were analyzed under joint research program between Waseda University and Moscow State University in 1990th. The statistics on single showers and families in present experiment is enough for a study on hadron interactions in exactly the overlapping region with the present collider experiments.

On the basis of the detailed study of our experimental set of events we elaborate way of analysis that can describe clearly the physics behind the observed families.

Correspondence to: Dr. V. Kopenkin (vvk@dec1.npi.msu.su)

2 Experimental setup

Pamir X-ray chamber has an area $10m^2$ and consists of 20 units, each of $0.5m^2$ size. The chamber is homogeneous in structure and uniform in detection efficiency of hadrons. Each unit of the 60 cm Pb chamber is a stack of 58 (59) X-ray emulsion films and 1 cm lead plates. The chamber thickness is ~ 3.5 nuclear mean free path. It allows detailed study of shower transition curve. The energy E of showers is estimated by measuring optical densities D at depths t and comparing with a calculation $D(E,t)$ based on the cascade theory.

3 Experimental statistics

We use in present analysis data from Pamir thick lead chambers $Pb68$, $Pb69$, $Pb72$, $Pb73$ of total exposure 57 m^2 year. The details are given in Table. 1.

Table 1. Experimental statistics on analyzed chambers

Item	Pb68	Pb69	Pb72	Pb73
Area (m^2)	8.5	7.5	10.	10.
Exposure ($year$)	1	1	2	2
Layers	58	58	59	59
Chamber (cm Pb)	60	60	60	60

4 Comparison with previous MSU data

We have made comparison of our experimental data (Waseda-MSU hereafter) using traditional method and the same selection criteria for identification of gamma rays and hadrons[1] and the same energy determination method as in previous Pamir and MSU experiments (Pamir collaboration , 1983; Rakobolskaya et al., 2000). Showers observed in X-ray chamber are classified into single that are not accompanied by any shower with energy above detection threshold E_{th} and family showers - bundle of parallel showers with the same zenith angle arrival direction. For family showers the energy-weighted center is determined, and energy of all γ-rays and hadrons within a circle of $R \leq R_{max}$ radius is calculated. The numerical data and comparison of family statistics are given in Table 2.

Table 2. Experimental statistics on families

Family	Experiment ($m^2 year$) chamber type	Flux
$100 \leq \Sigma E_\gamma \leq 500$ TeV	Pamir (84)	($m^2 year$)
$E_{th} = 4$ TeV		(0.4 ± 0.1)
$N_\gamma = 10$	Pb 40 cm	
$\Delta t = 6$ c.u.		
$R_{max} = 150$ mm	Waseda-MSU (57)	(0.4 ± 0.1)
	Pb 60 cm	
$\Sigma E_\gamma \geq 100$TeV		($m^2 year$)
$E_{th} = 6.3$ TeV	MSU (160)	(0.4 ± 0.1)
$N_\gamma = 4$		
$\Delta t = 6$ c.u.	Pb 40,60,110 cm	
$R_{max} = 150$ mm		
	Waseda-MSU (57)	(0.5 ± 0.1)
	Pb 60 cm	

In Fig. 1 we present differential energy spectra of gamma rays and hadrons in families 100 TeV $\leq \Sigma E_\gamma \leq$ 400 TeV with $E_{th} = 4$ TeV from Waseda-MSU experiment and MSU experiment (Rakobolskaya et al, 2000). As we can see there is good agreement between two experiments. Experimental characteristics on hadrons are presented in Table. 3. The observed hadron flux in present experiment is in agreement with the one previously reported by MSU group. Investigation of zenith angle distribution gives an attenuation mean free path of hadrons in the air for Pamir altitude as $105 \pm 6 g/cm^2$

This result is consistent with various studies made so far. The absorption of single and family hadrons in Pb using position of the hadron shower curve maximum

[1]Showers with $\Delta t \leq 6$ c.u. are considered to be gamma rays, all other are hadrons. Δt expresses the shift of depth of the shower maximum from the expected position of pure electromagnetic cascade.

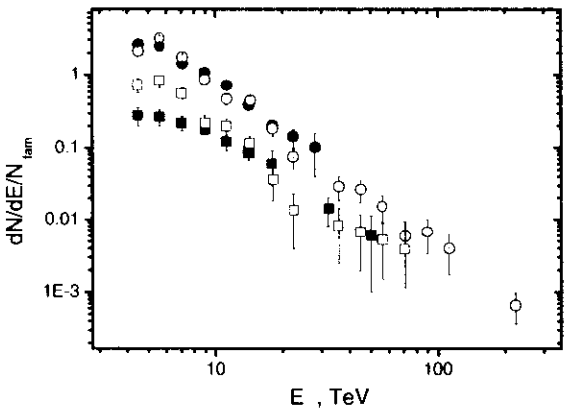

Fig. 1. Differential energy spectra of gamma rays and hadron in a family 100 TeV $\leq \Sigma E_\gamma \leq$ 400 TeV with $E_{th} = 4$ TeV. Marks are: open circles (gamma rays) and squares (hadrons) in Waseda-MSU experiment, solid circles and squares - gamma rays and hadrons from MSU experiment.

Δt at depths 22 – 78 c.u. is in good agreement with extensive study made with 110 cm Pb chamber.

Table 3. Experimental statistics on hadrons

Item	MSU	Waseda-MSU
Exposure $m^2 year$	30.5	57
Hadron flux $\times 10^{-10}$	(1.8 ± 0.2)	(1.8 ± 0.2)
$cm^2\ sec\ str$		
$E_{th} = 6.3$ TeV		
(single and family)		
Attenuation in air (g/cm^2)	(105 ± 7)	(105 ± 6)
(single and family)		
$E_{th} = 6.3$ TeV		
Absorption in Pb (g/cm^2)		
(single and family)	(212 ± 19)	(219 ± 13)
$E_{th} = 6.3$ TeV)		
$22 \leq \Delta t \leq 78$ c.u.		

5 Family study

The behaviour of families in the energy region above 100 TeV have been carefully studied by many authors with the purpose to get new information on hadron interactions. For example, families with $\Sigma E_{tot} = \Sigma E_\gamma + \Sigma E_h^{(\gamma)}$ in the range 100 – 1000 TeV provide information on hadron interactions and primary cosmic ray composition at primary energy $E_0 \sim 10^{15} - 10^{17}$ eV. Families are often classified into specific groups by their appearance or by their prominent features , such as content of gamma or hadron component ("gamma reach of hadron

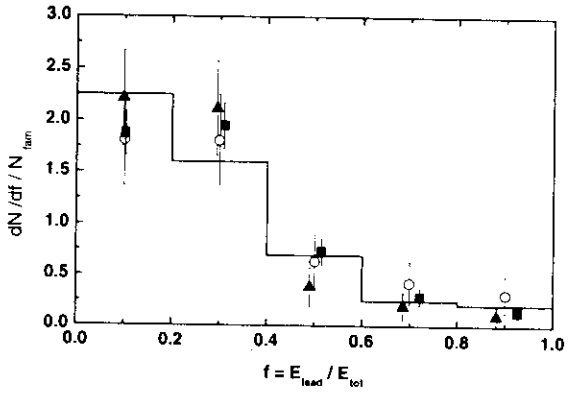

Fig. 2. Distribution of leading shower energy fraction in a family with $100 \leq \Sigma E_{tot} \leq 1000$ TeV. Marks are: open circles - Waseda-MSU experiment, triangles - Chacaltaya experiment, squares - Pamir carbon chamber experiment, solid line - UA5 simulation (normal primary composition).

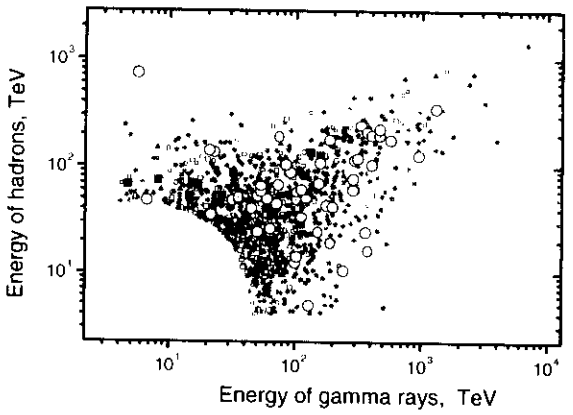

Fig. 3. Scatter plots of observed energy of hadrons $\Sigma E_h^{(\gamma)}$ and gamma rays ΣE_γ in Waseda-MSU experiment (open circles) and the UA5 simulation. Marks are: dots - proton, open squares - He, upward triangles - CNO, downward triangles - Mg, closed squares - Fe.

reach"), lateral spread ("wide or narrow"), multiplicity of showers ("large multiplicity or small multiplicity"), presence of clusters or halo ("family with halo, double core" and so on). Each family represents a certain pattern of showers. Once the feature of the family has been chosen, the pattern acquires its evaluation.

5.1 Leading shower in a family

To compare experimental data on gamma hadron families from different mountain experiments we have to choose some algorithm that would be almost free from experimental biases such as the altitude of the experimental site, details of the chamber structure, parameters of X-ray films and nuclear emulsions used, and the applyed methods of energy estimation and identification of showers. Taking into account the same trigger conditions for the selection criteria, let us consider the behaviour of the highest energy shower in a family, or leading shower, it can be either gamma or hadron.

In Fig. 2 we show distribution of the leading shower energy fraction $E_{lead}/\Sigma E_{tot}$ in families of $100 \leq E_{tot} \leq 1000$ TeV and $E_{th} = 4$ TeV from Pamir Pb chambers, Pamir Carbon chambers, and Chacaltaya experiment (Semba , 1983; Hasegawa et al., 1996) in comparison with the UA5 simulation (UA5 collaboration , 1987) results. Since we consider the ratio of energies E_{lead}/E_{tot}, this method is free from methodical details in each experiment. Fig. 2 shows that data from different experiments are consistent with each other and with simulation. It means that the average pattern of a family is similar in terms of showers in Chacaltaya and Pamir experiment.

Identification of showers as hadron or gamma or definition of an absolute energy scale in either of experiments could bring the very well known differences in observation of particular type of events with special characteristics. To study hadron characteristics in a family, it would be better to rely on analysis of data from the deep chamber with several m.f.p thickness that allows good separation of showers on gamma rays and hadrons.

6 Study of jets

To make arguments in a quantitative way let us express the pattern of energy flow of a family in terms of jet clusters, using step by step information on individual gamma rays and hadrons [2]. The scatter plot of observed energy of gamma rays ΣE_γ and hadrons $E_h^{(\gamma)}$ in families with $E_{tot} \geq 50$ TeV observed in Waseda-MSU experiment together with the result of the UA5 simulation, assuming normal primary composition, is shown in Fig. 3.

If the observed family has one collimated energy center it may be called a single core family. This core can be either surviving leading nucleon from proton primary, high energy air cascade, or cluster of gamma and hadrons. If the family spread is wide, with many local energy centers, it may be called a multi-core family and the heavy primary nucleus would be the best candidate.

By constructing jets we reveal the structure of the cascade complex and go "back" to main interaction and to the primary particle. In our analysis we have applied the following algorithm for experimental and simulation events: 1) decascading of gamma showers to gamma clusters with parameter $Z_{dec} = 11.0$ TeVmm

[2] For this purpose we applyed our new method of identification of gamma rays and hadrons (Fujimoto , 2000). This method takes into account the shape of transition curve and does not depend on $\Delta t = 6$ c.u. selection criterion

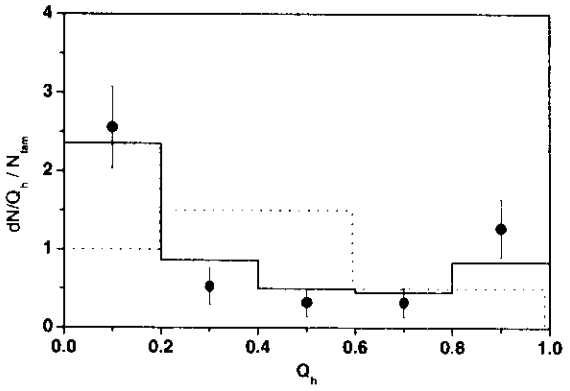

Fig. 4. Distribution of the hadron energy fraction Q_h inside of leading jet. Marks are: closed circles - experiment; solid line - proton simulation, dash line - Fe simulation.

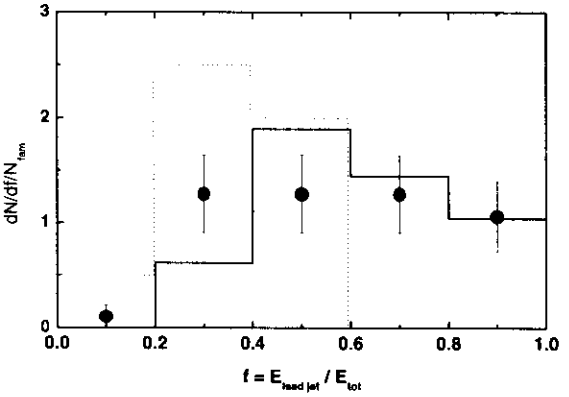

Fig. 5. Distribution of the leading jet energy fraction $f = E_{jet}/E_{tot}$. Marks are: closed circles - experiment; solid line - proton simulation, dash line - Fe simulation.

(Bayburina et al., 1981); 2) jet-clustering of all showers, clusters, hadrons and gamma rays with parameter Z_{jet} = 200 TeVmm; 3) normalizing jet energy by setting threshold $f'_{min} = 0.04$ for their fractional energy $f = E_{jet}/E_{tot}$. Parameters Z_{dec} and Z_{jet} reflect average transverse momentum in electromagnetic and strong interaction processes. In our analysis jet (in experiment and simulation) does not always represent the parent atmospheric interaction. It also includes successive interactions in the atmosphere by hadrons from parent interactions.

Fig. 4 shows distribution of hadron energy fraction Q_h inside of leading jet. This distribution is similar to the well known correlation between Q_h and number of hadrons in a family N_h. The peak near $Q_h \sim 0$ shows leading cluster of gamma showers or old cascade from a family started at high altitude. One peak is situated near $Q_h = 1$ and represents leading cluster of hadron nature or surviving nucleon. Families of experiment and simulation agree well and show that jets we have constructed are close to the initial stage of a family.

6.1 Leading jet

The main stream of energy flow in the atmospheric nuclear electromagnetic cascade is represented by leading jet. Energy fraction carried by leading jet shows signature of primary particle origin and surviving nucleon in interaction. Fig. 5 gives distribution of leading jet fractional energy $f = E_{lead}/E_{tot}$ in experiment (open circles) and simulation (proton - solid line and heavy - dash line). Value $f > 0.6$ corresponds to the families with clear energy center. The rest of the distribution shows families with several energy centers. Proton primary families show substantially large number of families with clear energy center. Families of heavy origin show absence of collimated energy concentration as we can see in Fig. 5. There is clear agreement between experiment and simulation based on primary proton dominant composition (normal composition) in energy region $E_0 \sim a\,few$ PeV, near the "knee".

7 Discussion and Conculsions

We show validity of our experimental data using conventional methods and get the same characteristics previously reported by MSU. With the concept of highest energy shower in a family we find no difference in a family pattern observed by X-ray chambers. In our consideration of families we studied pattern of energy flow represented by jets. We can conclude that general characteristics of cosmic ray families in the range 100-1000 TeV are compatible with predictions of simulation model based on accelerator experiment extrapolation to higher energies.

Acknowledgements. We are grateful to all the members of Pamir-Chacaltaya cosmic ray collaboration. Present study had been made during stay of V.Kopenkin in Institute for Cosmic Ray Research, University of Tokyo, as a research fellow of COE. He is deeply indebted to staff of ICRR for the hospitality and versatile and kind support.

References

Pamir collaboration, Proc. 18th ICRC, Bangaloure, Vol. 5, p.420, 1983.
Rakobolskaya, I.V. et al., Peculiarities of super high energy hadron interactions, MGU press, Moscow, p.256, 2000.
UA5 collaboration, Nucl. Phys. B, 29, 445, 1987.
Fujimoto, Y. et al. , Nucl. Phys. Proc. suppl. 97: 154, 2001.
Semba, H. , Prog. of Theor. Phys., Vol. 75. 111, 1983.
Hasegawa, S. et al., Nucl. Phys. B 474, 141, 1996.
Bayburina, S.G. et al. , Nucl. Phys. B 191, 1 , 1981.

Proceedings of ICRC 2001: 1 © Copernicus Gesellschaft 2001

ICRC 2001

Study of high energy cosmic ray interactions and primary composition using mountain based detectors

Y. Fujimoto[1], V. Kopenkin[2], A. Ohsawa[2], M. Tamada[3], C.E. Navia[4], and C.R.A. Augusto[4]

[1] Advanced Research Institute for Science and Engineering, Waseda University, 3-4-1, Okubo, Shinjuku-ku, Tokyo 169, Japan.
[2] Institute for Cosmic Ray Research, University of Tokyo, Kashiwa-no-ha 5-1-5, Kashiwa, Chiba 277-8582, Japan
[3] Faculty of Science and Engineering, Kinki University, Osaka, 577-8502, Japan
[4] Instituto de Fisica, Universidade Federal Fluminense, 24020-130 Niteroi, Rio de Janeiro, Brazil

Abstract. We report new experimental results obtained by MSU-Waseda collaboration. Our detector is 60 cm thick lead X-ray emulsion chamber exposed to cosmic rays at Pamirs. We show that this experiment can detect cosmic rays in the wide energy range $10^{13} - 10^{17}$ eV. Using experimental data we discuss the primary cosmic ray composition and the features of hadron interactions in the region before and after the "knee".

1 Introduction

At present accelerators reached energy region that is overlapped with the one studied by cosmic rays experiments using X-ray emulsion chambers. Naturally the main interest turned to the problems of origin and propagation of highest energy cosmic ray particles. At the same time there has not been reached consistent understanding on the phenomena observed by experiments with X-ray emulsion chambers. There are many results that could not find explanation within framework of present models (Lattes et al., 1980; Baradzei et al., 1992; Hasegawa et al., 1996) Here we present analysis based mainly on collaborative work of Moscow State University and Waseda University groups (Waseda-MSU hereafter) on joint study of experimental data obtained by Pb chambers exposed at Pamir. We have started our work with the motivation to have clear understanding on the measurement procedure and detector response. Based on this we have developed underlying phenomenological picture of physics that lies behind the gamma hadron families observed in X-ray chambers. To check the conclusions and get better view we used simulation calculations, the UA5 model[1].

Correspondence to: Dr. V. Kopenkin (vvk@dec1.npi.msu.su)

[1]The UA5 program (Tamada , 1994) is a simulation code based on phenomenological model of multiple particle production observed by CERN $p\bar{p}$ collider by UA5 collaboration experiment (UA5 collaboration, 1987). The energy distribution of produced particles shows violation of Feynman scaling law.

Before starting the classification of the observed events as anomalous we have to show how the general average picture of the physical object of interest looks like. We show that using simple quantities derived from experiment with mountain based X-ray chambers and a few assumptions on behaviour of hadron interactions (basically it is nearly constant inelasticity $< K > \sim 0.5$ in the energy region of our interest), we arrive to the conclusions that give consistent explanation to many observed family characteristics and shows the features of particle interactions in the fragmentation region at energies up to 10^{17} eV. Also our analysis reveals the qualitative view on composition of primary cosmic rays in wide energy region before and after the "knee".

2 Instrument description

In this work we use Waseda-MSU data from thick Pb X-ray chambers exposed at Pamir in 1988-1991. X-ray films of total exposure $ST = 57 m^2 year$ have been analyzed in Japan by joint Waseda-MSU team (Kopenkin et al., 1997). Pamir Pb chamber has homogeneous structure (Pb plates interleaved with RT6M Russian made X-ray films) that allows to study longitudinal profile of gamma rays and hadrons at every 1 cm interval. Large thickness (60 cm Pb) corresponds to ~ 3.5 m.f.p. and uniform hadron detection efficiency is close to 1. In our experiment we have made complete scanning and measurements of total available area, analyzing all showers (both, of single and family arrival) with $E_{th} = 4$ TeV. This type of study was not possible in another experiments.[2]

[2]In Pamir carbon chambers there is no detailed information on longitudinal shower profile. In Chacaltaya experi-

3 Average shower transition curve

First we show how our detector works in distinguishing showers of electromagnetic and hadron nature. Fig. 1 presents the average shower transition curve constructed over all observed single and family showers with $E_{th} = 4$ TeV.[3] The peak at small depths corresponds to the showers of gamma ray origin and the tail at larger depths reflects showers of hadron origin[4]. The value of attenuation of hadrons λ_{att} can be estimated from the exponential slope of the tail $\sim exp(-t/\lambda_{att})$. The experimentally observed λ_{att} obtained from the average $< D >$ transition curve is $248 \pm 30 g/cm^2$ and $343 \pm 40 g/cm^2$ for single and family showers respectively. Let us assume that majority of single showers are nucleons and majority of family showers are pions and apply well known formula that connects collision mean free path λ_{col} and λ_{att} given by $\lambda_{att} = \lambda_{col}/(1 - < (1-K)^{\alpha} >)$, where K is inelasticity and α is the power index of the energy spectrum of hadrons incident upon the chamber.

The power spectrum of single hadrons in our experiment is $\alpha = 2.0 \pm 0.1$ and of family hadrons - $\sim 1.2 \pm 0.1$. If $< K >= 0.5$, then these values appear to be in agreement [5] with the ones from formula as can be seen in Table. 1.

4 Hadrons in a family

The type of emulsion chamber used in Waseda-MSU experiment is particularly suitable for observation of hadron-gamma families. The comparison with the UA5 simulation results on hadron energy fraction in a family 100 TeV $\leq \Sigma E_{tot} \leq$ 1000 TeV is shown[6] in Fig. 2. The observed energy of the shower $E_h^{(\gamma)}$ induced by a hadron of energy E_h depends on the energy fraction of the electromagnetic component produced in the interaction $k_\gamma = \Sigma E_\gamma / E_h$. The experimental distribution has a best fit if we assume $< k_\gamma >= 0.15$. As we can see, this value is consistent with $< K >= 0.5$, which results in $< k_\gamma > \sim 1/6$ assuming pion multiple production mechanism. We have used these experimental values as an input in our simulation of families detected in Pb chamber.

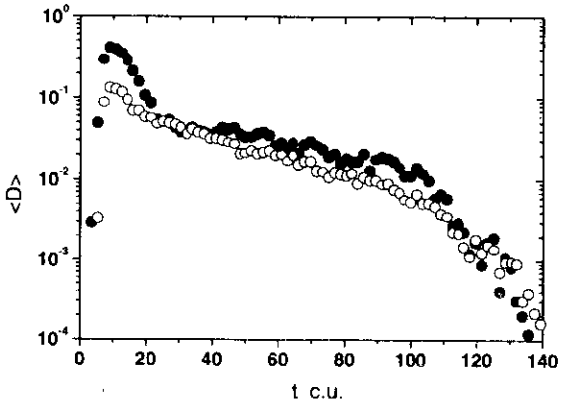

Fig. 1. Average shower transition curve ovel all observed single (open circles) and family (closed circles) showers with $E_{th} = 4$ TeV.

5 Lateral distribution of energy flow

The identification of showers as gamma rays or hadrons play a significant role in the study of families. There is an alternative way to describe the family development, using all showers without their identification as gamma rays or hadrons. In Fig. 3 we show the lateral distribution of energy flow of showers $d(\Sigma E_{tot})/2\pi R dR$ in the families from different energy regions: 58 families of $100 \leq \Sigma E_{tot} \leq 1000$ TeV from our Waseda-MSU experiment, 10 superfamilies 100 TeV $1000 \leq \Sigma E_{tot} \leq 7000$ TeV of $500\, m^2\, year$ exposure detected in deep Pb chambers of 40−110 cm thickness (Arisawa et al., 1994) , 4 superfamilies $1000 \leq \Sigma E_{tot} \leq 5000$ TeV from Chacaltaya experiment (Hasegawa et al., 1996) , and the highest energy family Tajikistan (Ohsawa , 1997) ($\Sigma E_{tot} \geq 50000$ TeV) detected in deep carbon chamber in Pamir experiment ($\sim 2.7\, \lambda_{int}$). For comparison we show results of the UA5 simulation for proton primary. It is clear that the same energy density flow can be created either by primary proton or by primary nuclei of higher energy (respectively to mass number A).

No significant difference is seen between experimental data on families from Pamir and Chacaltaya experiment when we use the same energy intervals and showers are not classified into gamma or hadrons. It shows that in terms of energy flow, lateral and longitudinal behaviour of family development observed by X-ray chambers are basically the same. Because of the large halo area in the center, the energy flow density of Tajikistan family is presented by individual showers outside the halo region. We can notice similarity in behaviour of families in terms of energy flow of showers in a broad energy region from

ment the chamber thickness is ~ 1 m.f.p. Also in previous set up of experimental study using Pb chambers of different thickness, the analysis has been performed either on single showers, or family showers, or both categories together, without their classification into two.

[3] We use as E_{th} the value usually accepted by Pamir Collaboration. Our conclusions are the same if we use, for instance $E_{th} = 6.3$ TeV or $E_{th} = 10$ TeV.

[4] Sharp decrease after 100 c.u. is due to the limited chamber depth. $1 c.u. = 0.56$ cm Pb.

[5] Experimentally measured values on *short* mean free path of family hadrons (Arisawa et al., 1994) and on *long* mean free path of single and family hadrons together, (Rakobolskaya et al., 2000) were obtained with another methodical procedure using the shift of depth of shower maximum.

[6] $\Sigma E_{tot} = \Sigma E_\gamma + \Sigma E_h^{(\gamma)}$.

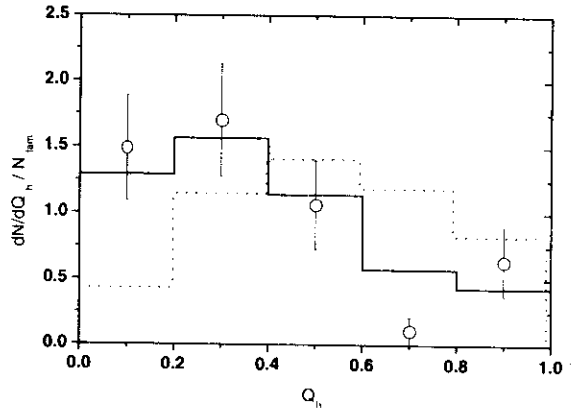

Fig. 2. Distribution of hadron energy fraction $Q_h = \Sigma E_h^{(\gamma)}/(\Sigma E_\gamma + \Sigma E_h^{(\gamma)})$ inside a family of $100 \leq \Sigma E_{tot} \leq 1000$ TeV. Marks are: open circles - experiment, solid line - simulation with $< k_\gamma >= 0.15$, dash line - simulation with $< k_\gamma >= 0.27$.

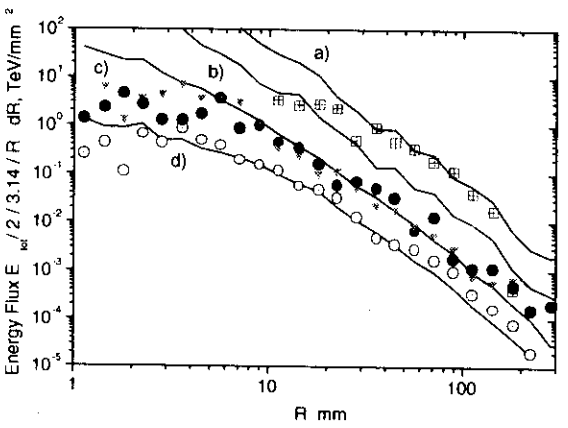

Fig. 3. Lateral distribution of energy flow density of showers ($E_{th} = 4$ TeV) in families. Marks are: open circles - family of $100 \leq \Sigma E_{tot} \leq 1000$ TeV (Waseda-MSU), closed circles - 1000-7000 TeV (MSU), squares - family Tajikistan, downward triangles - $1000 \leq \Sigma E_{tot} \leq 5000$ TeV (Chacaltaya). Solid lines - proton simulation (*a*) - $\Sigma E_{tot} = 200000$ TeV, *b*) - $\Sigma E_{tot} = 30000$ TeV, *c*) - $\Sigma E_{tot} = 3000$ TeV, *d*) - $\Sigma E_{tot} = 250$ TeV.

100 TeV until $\sim$ 50000 TeV in air and in the chamber[7].

5.1 Halo phenomenon

We can notice that the halo formation naturally can find its explanation from this picture. Halo is created when the energy flow is reached certain threshold. From two particles of the same energy and different mass number (for instance proton and iron), the lighter one (proton) is more efficient for halo creation (high energy density in the center). High energy nuclei in turn will be more efficient in creation of multiple halo of small size (due to many nucleons). As can be seen from Fig. 3 the energy density of family ($R \leq 10$) mm in interval $100 - 1000$ TeV is not enough to create sufficient condition for large halo formation, so halo is rarely observed. Superfamily region $\sim$ $1000 - 7000$ TeV is known for families with and without halo accompaniment. At very high energies, $E_{tot} \geq 10000$, TeV all families will be accompanied by halo in its center. These conclusions that follow from simple picture clarified by simulation, have found their confirmation in experimental observation (Pamir collaboration , 1991).

6 Total energy of family ΣE_{tot}

In order to study family characteristics in different energy intervals we have to use the same scale for family energy determination. The total energy of a superfamily with halo can be expressed as $\Sigma E_{tot} = E_{halo} + E_{out-halo}$.[8] The energy of halo [9] usually is estimated from the total track length as $E_{halo} = \epsilon * \int N_e(t)dt$, assuming the critical energy in Pb as $\epsilon = 7.4$ MeV

In experiment energy outside of halo region is determined as $E_{out-halo} = \Sigma E_\gamma + \Sigma E_h^{(\gamma)}$, with $E_{th} = 4$ TeV. Obviously, that halo region contains showers above and below this threshold E_{th}.

Comparing experimental and simulated lateral distribution of energy flow in the region outside of halo in a particular family, we can estimate the total energy of a family including halo region using the same energy threshold E_{th}. An upper limit on total energy of a family with $E_{th} = 4$ TeV is set by an experimental estimation of ΣE_{tot}, where halo energy E_{halo} is estimated from the raster scanning.

To choose between several variants we can use additional information on hadrons detected in the region outside of halo[10] From correlation on number of hadrons in a family N_h observed in the region $10 \leq R \leq 100$ mm (family can be either with or without halo) and the to-

[7] If there were a fraction of exotic type of process that becomes dominant with increasing energy, then the signal would have appear in the behaviour of highest energy shower or family pattern.

[8] obviously, "ordinary" family without halo in energy interval $100 \leq \Sigma E_{tot} \leq 1000$ TeV has $E_{halo} = 0$.

[9] The darkness D for every element in density matrix obtained after scanning of halo area is converted into electron density ρ by the characteristic curve of the X-ray film ($D = D_0(1 - exp(-\alpha\rho))$, The lateral distribution of electron density is integrated for every level to obtain the total number of electrons N_e in the halo.

[10] This is also important from the methodical point of view. Individual cascades form hadrons will be not masked by diffused dark halo area.

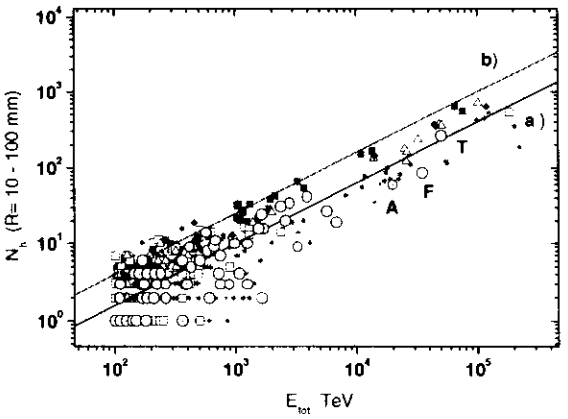

Fig. 4. Correlation of number of hadrons N_h in the region $10 \leq R \leq 100$ mm from the family center , and total family energy ΣE_{tot} with $E_{th} = 4$ TeV in simulation and experiment. Marks are: open circles - Waseda-MSU, closed circles - MSU, circle with A - family Andromeda (Yamashita , 1984), circle with F - family FIANIT (Pamir collaboration , 1984), circle with T - family Tajikistan, dots - proton, squares - Fe, open triangles - CNO, rhombuses - Mg. Line *a*) - $\sim A \times (E/A)^{0.8}$ for A=1, Line *b*) the same for $A = 56$.

tal energy of a family ΣE_{tot} shown in Fig. 4, the most probable mass number of primary particle, and correspondingly ΣE_{tot} can be estimated.

7 Primary composition

In our study of jets we have shown that of the families of 100-1000 TeV observed by emulsion chambers at mountain altitudes such as the Pamirs are induced by protons. The atmosphere plays the role of a filter for heavy component. Our experimental data (Fig. 4) in this energy region agree with assumption of normal chemical composition. These families are originated by cosmic rays with average primary energy $E_0 \sim$ *a few* PeV that is just near the "knee" region.

If the fraction of heavy nuclei increases in primary sepctrum, then the relative number of families originated by protons decreases. It can be seen that the relative number of families originated by nuclei (area between line[11] a) and line b)) increases with ΣE_{tot} and at higher energies (in emulsion chambers it corresponds to superfamilies of ($\Sigma E_{tot} \sim 1000 - 7000$,) TeV after the "knee" the primary composition becomes heavier, enriched with nucleus. We also show in Fig. 4 highest energy event Andromeda ($\Sigma E_{tot} \sim 20000$ TeV) detected in Chacaltaya experiment, and two highest energy events from Pamir $\sim 5000\, m^2\, year$ exposition - FIANIT ($\Sigma E_{tot} \sim 30000$ TeV) and Tajikistan. The energy of primary particle responsible for creation of these events (estimated by simultion) would be $E_0 \sim 10^{17} - 10^{18}$. It is important to note that primary cosmic ray at these energies contain protons.

8 Discussion and Conclusion

Using all available information from our experiment, we show the consistency of results with an assumption of $< K >= 0.5$ in hadron interactions in the energy region $10^{15} - 10^{17}$ eV[12]. We use a simulation calculation (using the same $< K >$) as a tool to check our experimental conclusions. We apply our method to the whole energy region studied by mountain chamber experiments and reveal the qualitatiove picture of primary cosmic ray composition before and after the "knee".

Table 1. Attenuation mean free path of hadrons with $E_h^\gamma \geq 4$ TeV. λ_{col} is assumed to be 190 g/cm^2 .

Hadron category	Spectrum index α	λ_{att} g/cm^2	λ_{att} ($< K >= 0.5$) g/cm^2
Single	2.0 ± 0.1	248 ± 30	253
Family	1.2 ± 0.1	343 ± 40	320

Acknowledgements. We are grateful to all the members of Pamir-Chacaltaya cosmic ray collaboration. Present study had been made during stay of V.Kopenkin in Institute for Cosmic Ray Research, University of Tokyo, as a research fellow of COE. He is deeply indebted to staff of ICRR for the hospitality and versatile and kind support.

References

Lattes, C.M.G. et al., Phys Rep. No.65, p. 151, 1980.
Baradzei, L.T. et al., Nucl. Phys. B 370,p. 365, 1992.
Hasegawa, S. et al., Nucl. Phys. B 474, p. 141, 1996.
Tamada, M., J. Phys. G:Nucl. Part. Phys. 20, 487, 1994.
UA5 collaboration, Nucl. Phys. B , 291, 445 , 1987.
Kopenkin, V. et al., Il Nuovo Cimento, Vol.19C, , p.1017, 1996.
Arisawa, T. et al., Nucl. Phys. B 424, p. 241, 1994.
Rakobolskaya, I.V. et al., Peculiarities of super high energy hadron interactions, MGU press, Moscow, p.256, 2000.
Ohsawa, A.. Il Nuovo Cimento, Vol 19C, p. 1031, 1997.
Pamir collaboration, Izevstiya AN SSSR, vol. 55, ser. fiz., p. 658, 1991.
Yamashita, S. et al., Proc. ISCRPF, Tokyo, p. 30, 1984.
Pamir collaboration, Proc. ISCRPF, Tokyo, p. 3, 1984.
Augusto, C.R.A. et al., Phys. Rev., D61, 012003, 2000.

[11] lines reproduce function $N_h \sim A \times (E/A)^{0.8}$

[12] We have to mention that our study of the inelasticity using the shape of transition curve of high energy hadrons produced similar result, $< K >\sim 0.6$ (Augusto , 2000).

Proceedings of ICRC 2001: 1 © Copernicus Gesellschaft 2001

ICRC 2001

Energy Distribution of Produced Particles in Multiple Particle Production based on Data of Direct Observation

Akinori Ohsawa[1], Edison H. Shibuya[2], and Masanobu Tamada[3]

[1]Institute for Cosmic Ray Research, University of Tokyo, Kashiwa, Chiba, 277-8582 Japan.
[2] Instituto de Fisica Gleb Wataghin, Univ. Estadual de Campinas, 13083-970 Campinas, São Paulo, Brasil.
[3]Faculty of Science and Technology, Kinki University, Higashi-Osaka, Osaka, 577-8502 Japan.

Abstract. The energy distribution of produced particles in multiple particle production is formulated empirically based on the data of direct observations by accelerator and cosmic-ray experiments at $10^{12} \sim 10^{14}$ eV. The formulated distribution indicates violation of the Feynman scaling law, which was shown to be valid in low energy region of $\leq 10^{12}$ eV. That is, the particle density is suppressed in the forward region and enhanced in the central region, compared with the distribution of the Feynman scaling law. Consequences of the formulated distribution, such as multiplicity, inelasticity, etc., are discussed at high energies of $\geq 10^{15}$ eV by extrapolation. The distribution is also compared with those of nuclear interaction models which are used widely in simulations of accelerator and cosmic-ray experiments.

1 Introduction

To discuss multiple particle production (MPP) it is convenient to start from the energy distribution of produced particles, since some important features of MPP, such as inelasticity and multiplicity, are derived from it. To discuss the energy distribution, however, we have almost no *a priori* guiding principles except energy conservation. Hence it may be reasonable to take a phenomenological approach or to start from experimental data while as much as possible trying to avoid assumptions without experimental basis.

Our study is made in the following way. Assuming the energy distribution of produced particles, which tends to that of the Feynman scaling law at low energies, we determine magnitudes of the scaling violation parameters at various collision energies where the experimental data is available. Assuming that the obtained energy dependence of the scaling violation parameters is valid up to 10^{20} eV, we discuss the consequences of the formulated distribution at higher energies. The formulated distribution is compared with the predictions of models which are used widely in simulations in accelerator and cosmic-ray experiments.

Correspondence to: ohsawa@icrr.u-tokyo.ac.jp

2 Energy distribution of produced particles

In this section we discuss the energy distribution of produced particles in $N - N$ (nucleon−nucleon) inelastic collisions, under the assumption that the final state of multiple particle production consists of a surviving particle, which has the same particle nature as the incident particle, and the produced particles. The view is valid empirically if one assumes that the energy of the surviving particle is distributed between 0 and E_0 in the laboratory system. Note that the surviving particle is not always the leading particle or the highest energy particle. Plausibility of the assumption was discussed in detail (Augusto et al., 1999). This approach does not require specifying kinds of produced particles at all.

2.1 Scaling function

Feynman speculated that the energy distribution of produced particles in multiple particle production, expressed by the variable $x^* \equiv 2p^*_{\parallel}/\sqrt{s}$ ($p^*_{\parallel}$: the longitudinal component of the momentum vector $\boldsymbol{p}^*$ of the produced particle),[1] is independent of the incident energy $\sqrt{s}$ at high energies (Feynman, 1969). This assumption appeared to be valid up to the energy of $\sqrt{s} = 63$ GeV, the maximum available energy at that time (Taylor et al., 1976). One of the empirical formulae to express the energy distribution of charged produced particles is (Gaisser et

[1]The quantities with and without an asterisk (*) are those in the center of mass system and in the laboratory system, respectively.

al., 1978)

$$\frac{dN}{dx^*} \equiv \frac{1}{\sigma_{inel}} \frac{d\sigma}{dx^*} = D\frac{(1-x^*)^d}{x^*} \tag{1}$$

$$(D = (d+1)/3 = 1.67, \quad d = 4.0)$$

which is called 'the scaling function'.

2.2 Energy distribution at high energies

At still higher energies, there are several data sets of direct observation by cosmic-ray and accelerator experiments (Chinellato et al., 1983), (Alner et al., 1986), (Pare et al., 1990), (Haar et al., 1997). Note that the experimental data are presented in various quantities, such as rapidity density, pseudo-rapidity density, etc., owing to the experimental conditions of the respective groups.

To compare these data with the scaling function, one has to transform dN/dx^* into $dN/d\eta^*$, dN/dy^*, etc. In doing so, one has to take into account that the average value of the transverse momentum $< p_T >$ depends on the rapidity, *i.e.* the value becomes smaller in the forward region (Lattes et al., 1971). Hence we assume

$$\frac{dN}{dx^* dp_T} = aD\frac{(1-a'x^*)^d}{\sqrt{x^{*2} + \left(\frac{2\mu}{\sqrt{s}}\right)^2}}\, g(p_T) \tag{2}$$

$$(\mu \equiv \sqrt{p_T^2 + m_\pi^2})$$

where the parameters a and a' are adjustable. This formula reproduces the scaling function of eq.(1) using $a = a' = 1$ and $\sqrt{s} \to \infty$. The parameters a (≥ 1) and a' (≥ 1) express enhancement of the scaling function in the central region and suppression in the forward region, respectively.

The p_T-distribution is assumed to be

$$g(p_T)dp_T = p_T \exp\left(-\frac{p_T}{p_0}\right)\frac{dp_T}{p_0^2} \tag{3}$$

with

$$p_0 = \begin{cases} c & (x^* < x_0^*) \\ c\left(\frac{x_0^*}{x^*}\right)^{c'} & (x^* > x_0^*) \end{cases} \tag{4}$$

$$(c = 0.2\ \mathrm{GeV}/c, \quad c' = 0.57, \quad x_0^* = 0.08)$$

According to the p_T-distribution of eq.(3), the average value of p_T, $< p_T >= 2p_0$, becomes smaller in the forward region $x^* > x_0^*$, which is observed by the experiments (Lattes et al., 1971), (Pare et al., 1990).

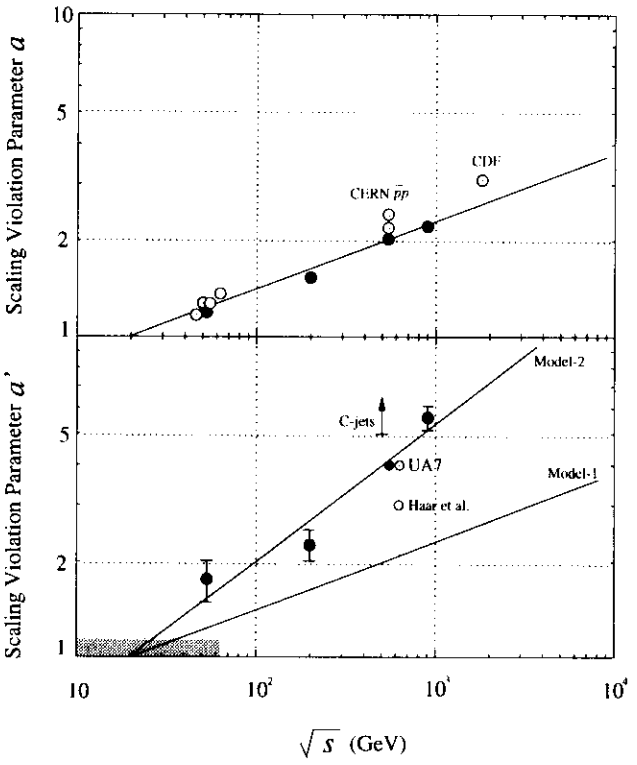

Fig. 1. Energy dependence of the scaling violation parameters, a (the upper figure) and a' (lower) in eq.(2) in the text. Plots are obtained by fitting the calculated curves of (pseudo-) rapidity density distribution to those of the experimental data. The full circles are from the experimental data of the UA5 Collaboration (Alner et al., 1986), and the open circles are from those of other experimental groups (Alner et al., 1986), (Abe et al., 1990), (Haar et al., 1997). The bar with an arrow, indicated as "C-jets", is from the cosmic-ray experiment (Chinellato et al., 1983). The hatched area indicates the energy region where the Feynman scaling law ($a \simeq 1.0$ and $a' \simeq 1.0$) is verified by the experiments. The lines are the assumed energy dependences in Model-1 and Model-2. is verified by the experiments. The lines are the assumed energy dependences in Model-1 and Model-2.

2.3 Scaling violation parameters

The above distribution (2) can be transformed into those of dN/dy^* and $dN/d\eta^*$ easily. Hence we can calculate the (pseudo-)rapidity density distribution at the incident energy $\sqrt{s}$ for various values of the parameters a and a', which are to be compared with those of the experimental data.[2]

We assume the energy dependence of parameter a as

$$a = \left(\frac{s}{s_0}\right)^\alpha \simeq \left(\frac{E_0}{A}\right)^\alpha \qquad (\alpha = 0.105) \tag{5}$$

$$(s_0 = 3.9 \times 10^2\ \mathrm{GeV}^2,\ A = 2.0 \times 10^2)$$

[2]The data are those of all inelastic events but not only NSD (non-single-diffractive) events. That is, $\sigma_{inel} = \sigma_{NSD} + \sigma_{SD}$.

The energy dependence of the parameter a is shown in Fig. 1 together with experimental data. Then the pseudo-rapidity density at $\eta^* = 0$ is given by

$$\left(\frac{dN}{d\eta^*}\right)_{\eta^*=0} = D < \frac{p_T}{\mu} > a = 1.67 \times 0.83 \times \left(\frac{s}{s_0}\right)^{\alpha} \quad (6)$$

which reproduces $\rho(0) = 0.74 s^{0.105}$ found by the UA5 Collaboration (Alner et al., 1986).

From the energy dependence of the parameters a and a' in Fig. 1, we assume two cases of

$$a' = \left(\frac{E_0}{A}\right)^{\alpha'} \qquad (\alpha' = 0.105 \quad \text{and} \quad 0.210) \qquad (7)$$

which are called Model-1 and Model-2 hereafter. The parameters a and a' in Model-1 have the same energy dependence, and those in Model-2 are the best-fit to the experimental data. Note that the data from Harr et al. and from the C-jets of the Chacaltaya experiment deviate from the line of Model-2. Model-0 with $a = a' = 1.0$, which stands for the case of Feynman scaling law, is included for reference.

To show how the experimental data are described by the formula of eq.(2) with appropriate values of the parameters a and a', Fig. 2 presents the pseudo-rapidity density distributions of all inelastic events (but not only of non-single-diffractive events) recorded by the UA5 Collaboration together with those of the formulated models. One can see in the figure that the reproduction is satisfactory by Model-2 and that Model-0 (the Feynman scaling law) cannot reproduce the data both in the central and forward regions. Note that the distribution of Model-0 is slightly energy-dependent, as can be seen in eq.(2).

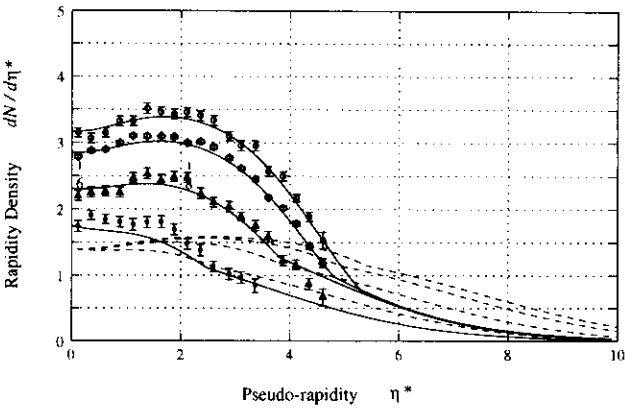

Fig. 2. Pseudo-rapidity density distributions by UA5 Collaboration experiment (plots), those of Model-2 (solid lines) and those of Model-0 (chain lines). The data are those of all inelastic events at the energies of $\sqrt{s} = 53$ GeV (•), 200 GeV (△), 546 GeV (◇), and 900 GeV (○). The solid lines are by Model-2 with the parameter values a' of the best-fitting at respective energies

3 Discussions

3.1 Multiplicity and inelasticity at high energies

Fig. 3 shows the energy dependence of charged multiplicity,

$$m(E_0) = \int_0^{1/a'} dx \int_0^{\infty} dp_T \frac{aD(1-a'x)^d}{\sqrt{x^2 + \left(\frac{2\mu}{\sqrt{s}}\right)^2}} \; g(p_T)$$

predicted by the formulated models. One can see in the figure that difference in the multiplicity is small between Model-1 and Model-2 because we have

$$m(E_0) \simeq a\left[\ln\frac{\sqrt{s}}{\mu} - \ln a'\right].$$

That is, the parameter a' appears in the form of $\ln a'$. It is no surprise that the energy dependence of Model-2 agrees better with the experimental data than that of Model-1.

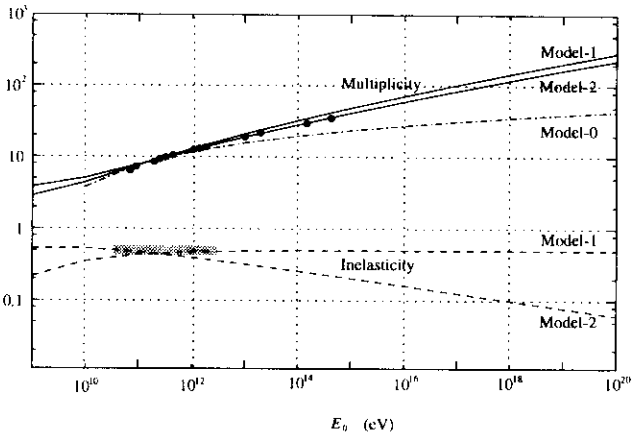

Fig. 3. Energy dependence of charged multiplicity and that of total inelasticity, predicted by the models. Experimental data of average charged multiplicity (full circles) is from bubble chambers, ISR and S$\bar{p}p$S, compiled in Ref. (Alner et al., 1986). The multiplicity is not different so much between Model-1 and Model-2. Model-2 describes the experimental data better than Model-1, because Model-2 has the best-fit parameters to describe the rapidity density distribution. Inelasticity is decreasing in Model-2, while it is constant (=0.5) for Model-0 and Model-1. The shadowed area indicates the region where the Feynman scaling law, *i.e.* $< K >= 0.5$, is verified by the experiments within the experimental errors.

Fig.3 shows also the energy dependence of the average total inelasticity in the laboratory system, defined by

$$< K > \equiv \frac{3}{2}\int_0^{1/a'} x dx \int_0^{\infty} dp_T \; aD \frac{(1-a'x)^d}{\sqrt{x^2 + \left(\frac{2\mu}{\sqrt{s}}\right)^2}} \; g(p_T)$$

It shows that the inelasticity decreases considerably in Model-2 at high energies while it is constant (*i.e.* 0.5)

in Model-0 and in Model-1.[3] It is worth noting that $< K >= 0.5$ holds when the relation $\alpha = \alpha'$ holds, irrespective of the values of α and α'.

3.2 Models used in simulations

It is also interesting to see how the formulated distribution is reproduced by the models which are used recently in simulations of atmospheric cosmic-ray diffusion. In Fig. 4 we compare the pseudo-rapidity density distributions (Knapp et al., 1996), predicted by UA5 code (Alner et al., 1986)[4], VENUS (Werner, 1993), QGSJET (Kalmykov and Ostapchenko, 1993) SIBYLL (Fletcher et al., 1994), HDPM (Capdevielle et al., 1992) and DPMJET (Ranft, 1995), with those of the present models. Note that the pseudo-rapidity density by simulations is for NSD (non-single-diffractive) events while that of the calculation is for all inelastic events.

The following observations can be made from Fig. 4.
(1) In the central region the distributions are similar except that of HDPM.
(2) In the middle region QGSJET, VENUS, DPMJET predict higher density appreciably than that of Model-2.
(3) In the forward region all the model predictions are almost consistent.
(4) UA5 code predicts the most consistent distribution with that of Model-2.[5]
(5) The difference of the rapidity densities, predicted by respective simulation models, is not negligibly small.
(6) The experimental data at Harr et al. is almost consistent with those by QGSJET. (See also the lower figure in Fig. 1.)
(7) The rapidity density of the QGSJET model, which is used frequently at present in simulations of cosmic-ray phenomena, is almost between those of Model-1 and Model-2.

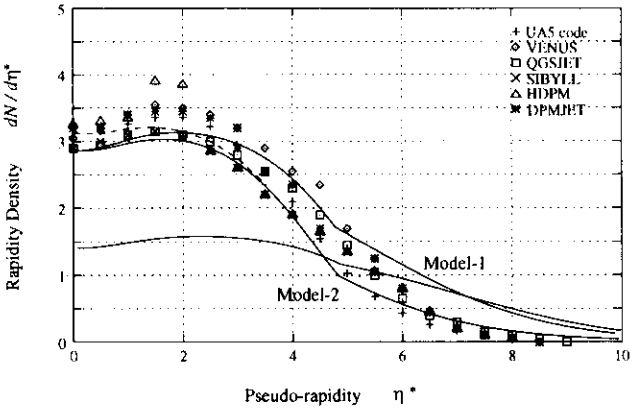

Fig. 4. Pseudo-rapidity density distributions at $\sqrt{s} = 546$ GeV. Plots are by the simulation models (UA5 code, VENUS, QGSJET, SIBYLL, HDPM and DPMJET). The data by the simulations are based on the NSD (non-single-diffractive) events, while those by Model-0, Model-1 and Model-2 (solid lines) are for all inelastic events. The chain line is that of Model-2 which is corrected for NSD events.

References

F. Abe et al. (CDF Collaboration), Phys. Rev. D41(1990) 2330.

G.L. Alner et al. (UA5 Collaboration), Z. Phys. C33 (1986) 1; Nucl. Phys. B291 (1987) 445; Phys. Rep. Nos.5 and 6 (1987) 247.

G.J. Alner et al. (UA5 Collaboration), CERN-EP/86-213 (1986).

C.R.A. Augusto, S.L.C. Barroso, Y. Fujimoto, V. Kopenkin, M. Moriya, C.E. Navia, A. Ohsawa, E.H. Shibuya, and M. Tamada, Phys. Rev. D61 (1999) 012003.

J.N. Capdevielle et al., Preprint of Kernforschungszentrum Karlsruhe KfK 4998 (1992).

J.A. Chinellato et al., Prog. Theor. Phys. Suppl. No.76 (1983) 1.

R. Feynman, Phys. Rev. Lett. 23 (1969) 1415.

R.S. Fletcher, T.K. Gaisser, P. Lipari, T. Stanev, Phys. Rev. D50 (1994) 5710; J. Engler, T.K. Gaisser, P. Lipari, T. Stanev, Phys. Rev. D46 (1992) 5013.

T.K. Gaisser, R.J. Protheroe, K.E. Turver, T.J.L. McComb, Rev. Mod. Phys. 50 (1978) 859.

R. Haar, C. Liapis, P. Karchin, C. Biino, S. Erhan, W. Hofmann, P. Kreuzer, D. Lynn, M. Medinnis, S. Palestini, L. Pesando, M. Punturo, P. Schlein, B. Wilkens, J. Zweizig, Phys. Lett. B401 (1997) 176.

N.N. Kalmykov, S.S. Ostapchenko, Yad. Fiz. 56 (1993) 105; N.N. Kalmykov, S.S. Ostapchenko, Phys. At. Nucl. 56 (3) (1993) 346; N.N. Kalmykov, S.S. Ostapchenko, A.I. Pavlov, Bull. Russ. Acad. Sci. (Physics) 58 (1994) 1966.

J. Knapp, D. Heck, G. Schatz, Preprint of Forchungszentrum Karlsruhe, FZKA 5828 (1996).

C.M.G. Lattes et al. Prog. Theor. Phys. Suppl. No.47 (1971) 1.

E. Pare, T. Doke, M. Haugenauer, V. Innocente, K. Kasahara, T. Kashiwagi, J. Kikuchi, S. Lazano, K. Masuda, H. Murakami, Y. Muraki, T. Nakada, A. Nakamoto, T. Yuda, Phys Lett. B242 (1990) 531.

J. Ranft, Phys. Rev. D51 (1995) 64.

F.E. Taylor, D.C. Carey, J.R. Johnson, R. Kummerud, D.J. Richie, A. Roberts, J.R. Sauer, R. Shafer, D. Theriot, J.K. Walker, Phys. Rev. D14 (1976) 1217.

K. Werner, Phys. Rep. 232 (1993) 87.

[3] It may look strange that the average inelasticity $< K >$ is 0.5 for Model-1, which has a higher rapidity-density than QGSJET (See Fig. 4.), since QGSJET found $< K > \simeq 0.6$. The effect is due to the difference in sampling of events, *i.e.* all inelastic events in the former and NSD events in the latter. In other words the average inelasticity by QGSJET is ~ 0.5 for all inelastic events.

[4] UA5 Collaboration made a simulation code which describes the data observed by the collaboration.

[5] The code does not necessarily predict the pseudo-rapidity density correctly in the forward region, because the observed pseudo-rapidity region by UA5 Collaboration is limited to $\eta^* \leq 4.5$.

Proceedings of ICRC 2001: 1 © Copernicus Gesellschaft 2001

ICRC 2001

A phenomenological model of multiple particle production and highest energy air showers.

Akinori Ohsawa[1], Edison H. Shibuya[2], and Masanobu Tamada[3]

[1]Institute for Cosmic Ray Research, University of Tokyo, Kashiwa, Chiba, 277-8582 Japan.
[2]Instituto de Fisica Gleb Wataghin, Univ. Estadual de Campinas, 13083-970 Campinas, São Paulo, Brasil.
[3]Faculty of Science and Technology, Kinki University, Higashi-Osaka, Osaka, 577 Japan.

Abstract. The energy distribution of produced particles in multiple particle production, which is formulated empirically based on the direct observation data by accelerator and cosmic-ray experiments, shows violation of the Feynman scaling law with decreasing inelasticity at high energies. We show that the extrapolation of the formulated distribution does not describe the highest energy ($\sim 10^{20}$ eV) air showers. We also discuss how large the ambiguity is in the energy determination of highest energy air showers, due to limited information on nuclear interaction characteristics at high energies.

1 Introduction

We formulated empirically the energy distribution of produced particles in multiple particle production, based on the data of direct observation by accelerator and cosmic-ray experiments in the energy region $10^{12} \sim 10^{14}$ eV. (Ohsawa et al., 2000)

The formulated energy distribution shows that the Feynman scaling law, which is shown to be valid in the energy region below $\sqrt{s} = 63$ GeV, is violated appreciably both in the central region and in the forward region at high energy. That is, the particle production is enhanced in the central region and suppressed in the forward region. And the suppression in the forward region is stronger than the enhancement in the central region. Consequently the total inelasticity $< K >$ becomes smaller than 0.5 appreciably at high energy. It is also shown that the nuclear interaction models, which are assumed in the recent calculations to simulate the cosmic-ray diffusion in the atmosphere, are not compatible with the formulated energy distribution.

In the present paper we discuss whether the formulated energy distribution is compatible or not with the data of extremely high energy ($\sim 10^{20}$ eV) air showers. The energy dependence of nuclear interaction characteristics appears in most distinct way at these energies.

Correspondence to: ohsawa@icrr.u-tokyo.ac.jp

2 Diffusion of Cosmic rays in the atmosphere.

2.1 Air showers

A high energy primary cosmic-ray proton, incident upon the top of the atmosphere, makes a nuclear collision with an atmospheric nucleus, and many particles — one surviving particle and a number of produced particles — are produced through the collision. The surviving particle, either a proton or a neutron, repeats inelastic collisions in the atmosphere. The inelastic cross section of the nucleon-air collision increases with the incident energy.

The produced particles are assumed to be pions. The energy distribution of produced pions is substituted by that of $N - N$ collision, which is formulated by us (Ohsawa et al., 2000), because the effect of the air nucleus target appears only in the backward region.[1] The charged pions among the produced pions make nuclear collisions in the atmosphere again. The collision mean free path of charged pions has the same energy dependence as that of nucleon. We neglect decays of charged pions into muons.

The multiple particle production, induced by a charged pion, has essentially the same characteristics as the one by a nucleon, which is confirmed within the errors of the experimental data in low energy region. (Gaisser et al., 1978)

That is, the final state of the collision consists of one surviving pion and produced pions whose energy distribution is the same as the one of proton collision. The differences are that the inelastic cross section of pion is

[1]The diffusion of cosmic rays in the atmosphere is governed by the high energy particles, produced in the forward region.

Table 1. Energy dependences of the scaling violation parameters

Model	α	α'	$< K >$	Remark
Model-0	0	0	0.5	
Model-1	0.105	0.105	0.5	
Model-2	0.105	0.210	$0.5(E_0/A)^{-0.105}$	the best-fit

smaller than that of proton, and that the surviving pion has a probability to be a neutral pion (called the 'charge exchange' process).

The neutral pions among the produced pions and those through the charge exchange process decay into γ-rays which produce a number of electromagnetic component, electrons and photons, via electromagnetic cascade process.

2.2 Assumptions for elementary processes

Following the above scenario we formulate the elementary processes.

(1) Inelastic collision mean free path

We formulate the energy dependence of the mean free paths of $N - air$ and $\pi - air$ collisions in the following way. (Nam et al., 1983), (Hara et al., 1983), (Dyakonov et al., 1987)

$$\lambda_N(E_0) = \lambda_N \left(\frac{E_0}{B}\right)^{-\beta} \qquad \lambda_\pi(E_0) = \lambda_\pi \left(\frac{E_0}{B}\right)^{-\beta} \quad (1)$$

$$(\lambda_N = 80.0\ \mathrm{g/cm^2},\ \lambda_\pi = 113\ \mathrm{g/cm^2},\ \beta = 0.056)$$

(2) Energy distribution of produced particles

The energy distribution of produced charged particles in multiple particle production is formulated in our paper. (Ohsawa et al., 2000) In the laboratory system it is

$$\varphi(E_0, E)dE = D\left(\frac{E_0}{A}\right)^{\alpha}\left[1 - \left(\frac{E_0}{A}\right)^{\alpha'}\frac{E}{E_0}\right]^{d}\frac{dE}{E} \quad (2)$$

$$(A = 2.0 \times 10^2\ \mathrm{GeV},\ D = 1.67,\ d = 4.0)$$

where E_0 is the energy of the incident particle. The parameters α and α' are tabulated in Table 1. The values of Model-2 are the best-fit to the experimental data, and Model-0 and Model-1 are for reference.

(3) Inelasticity

According to eq.(2) the average total inelasticity is given by

$$< K > \equiv \frac{3}{2}\int_0^{E_0} E\varphi(E_0, E)dE = 0.5\left(\frac{E_0}{A}\right)^{\alpha-\alpha'}$$

That is, the average inelasticity decreases with the incident energy for Model-2.

We assume that the inelasticity K is distributed uniformly between 0 and $2 < K >$ (≤ 1.0). The distribution has the average value of the inelasticity $< K >$.

(4) Charge exchange probability of the surviving pion is assumed to be $b = 0.3$.

Table 2. Cases to be discussed

Case	α and α' in eq.(2)		Cross section	Remark
	α	α'		
A	0	0	$\beta = 0$	$b = 0$ and
	(the scaling law)		(constant)	$b = 0.3$
B	0	0	$\beta = 0.056$	
	(the scaling law)		(increasing)	
C	0.105	0.105	$\beta = 0$	Model-1
	(the law violated)		(constant)	
D	0.105	0.210	$\beta = 0$	Model-2
	(the law violated)		(constant)	

3 Air shower size

As can be seen in Appendix A, one can calculate the air shower size N_e if one can solve the diffusion equations for nucleon and pion components. It is not simple, however, to solve them taking all the processes, mentioned above, into account simultaneously. Therefore we discuss the effects of respective processes one by one. That is, we calculate the cases, tabulated in Table 2, and discuss the ratio between the air shower size of each process and that of the case A.

Fig. 1 shows the transition curve of the air shower size of the case A for the primary proton with the energies $E_0 = 10^{18}$, 10^{19}, and 10^{20} eV. (See Appendix A.) One can see in the figure that the air showers of 10^{20} eV are at the maximum development at sea level and that the relation $E_0/N_e \simeq 2.0$ (GeV) holds approximately, irrespective of the primary energy E_0.

The effect of the charge exchange process is examined, too, assuming the probability $b = 0.3$. The effect is almost constant over the atmospheric depth, amounting 13 %, as can be seen in Fig. 2. The approximately constant effect over the depth can be explained by the facts; (1) that the probability b is included in the attenuation mean free path of pion component $\xi\mu_\pi(s)$ and in the coefficient of the pion term, in such ways that the attenuation of the air shower size becomes faster and that the size becomes larger, respectively, and (2) that the shower development before the shower maximum is governed by $e^{\xi_0\lambda_1(s)z}$ but not by $e^{\xi\mu_\pi(s)z}$. (See Appendix A.)

Fig. 2 shows the ratio of the air shower size between the cases B, C and D and the case A, tabulated in Table 2, at the primary energy $E_0 = 10^{20}$ eV. One can see the following in the figure.

(1) Effect of the charge exchange process of the surviving pion is almost constant over the atmospheric depth, and amounts 13 %.

(2) Effect of increasing cross section is large at high altitude, but is small at sea level. (This tendency can be seen by the analytic expression of the air shower size where the increasing cross section is taken into account.)

(3) The effects of scaling violation, in Model-1 and in Model-2, have similar depth dependence, but the abso-

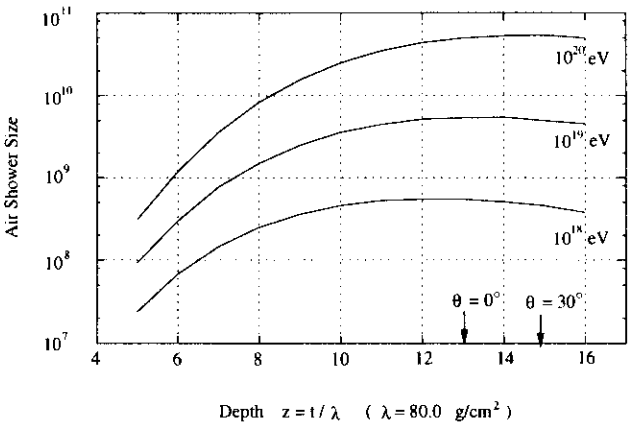

Fig. 1. Transition curve of the air shower size for the primary proton with the energy $E_0 = 10^{18}$, 10^{19} and 10^{20} eV, for Case A (Model-0 and constant cross section). The arrows indicate the depth of the sea level (1,030 g/cm^2) for the air showers with the inclination $\theta = 0°$ and 30°.

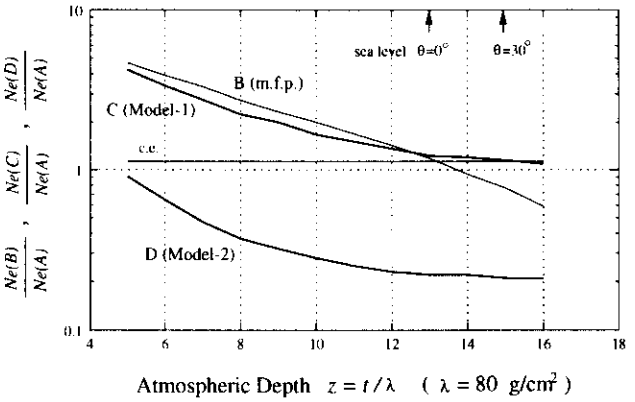

Fig. 2. Ratio of air shower size, N_e(B)/N_e(A), N_e(C)/N_e(A) and N_e(D)/N_e(A), along the depth. The cases of A, B, C and D are tabulated in Table 2. The primary energy of a proton is 10^{20} eV.

lute values of them differ by five times.
(4) Model-2 gives smaller air shower size, and the attenuation of the air shower size after the shower maximum is very slow due to the small value of inelasticity.
(5) At sea level the air shower size is affected in the greatest manner by the difference of the nuclear interaction model, among the examined processes of nuclear interacxtion characteristics.

4 Summary and discussions

(i) Analytical expression is given for the air shower size, based on the formulated models of nuclear interactions. It enables us to discuss how the physical processes — the charge exchange of the surviving pion, increasing cross section of *hadron − air* collisions, and the energy distribution of produced particles — affect the air shower size. These processes are the major factors to govern the diffusion of high energy cosmic rays in the atmosphere. We obtained the following observations about the size of the extremely high energy air showers.
(1) Effect of charge exchange process is almost constant (×1.13) over the whole depth in the atmosphere.
(2) Effect of increasing cross section is large (× 2 ∼ 3) at mountain altitudes, but small (×1.18) at the sea level.
(3) Effect of scaling violation of Model-1 is large (× 2 ∼ 3) at mountain altitudes, but small (×1.23) at sea level.
(4) Effect of scaling violation of Model-2 is not negligible at any depth, i.e. × 0.6 ∼ 0.4 at mountain altitudes and ×0.22 at the sea level.

(ii) The air shower size at sea level, expected by the present calculation, is tabulated in Table 3 for the incident proton of $E_0 = 10^{20}$ eV. In the table the effects of the charge exchange process and the increasing cross section are obtained by Fig. 2. To calculate the expected air shower size, to which the effects of charge exchange probability and increasing cross section are included, we multiplied all the factors because the factors are close to 1.0.

(iii) M. Nagano et al. examined the method of energy determination of extremely high energy air showers, employed by AGASA experiment, by the simulation code of CORSIKA (Capdevielle et al., 1992)(with QGSJET model). And they reached the conclusion that the method works well for the highest energy air showers. (Nagano et al., 1998) The simulation gives $N_e = 5.5 \times 10^{10}$ for the proton-induced air showers of $E_0 = 10^{20}$ eV.[2] We can see the following points by comparing the value with those in Table 3.
(1) The value by the simulation is between those of Model-1 and Model-2. In this sense our calculation and the simulation are consistent each other, because we saw in our paper (Ohsawa et al., 2000) that the pseudo-rapidity density distribution by the QGSJET model is between those by Model-1 and Model-2.
(2) If we take Model-1, the energy spectrum of highest energy air showers shifts to the left (lower energy side) by a factor 1.5.
(3) If we take Model-2, which is the best-fit to the experimental data, the energy spectrum shifts to right (higher energy side) by a factor 3.7.

One can see that the energy distribution of produced particles has the largest effect on the size of extremely high energy air showers among the physical processes, discussed in this paper. Hence we have to specify the energy distribution of produced particles in multiple particle production in more detail, in order to confirm the extremely high energy cosmic rays exceeding 10^{20} eV.

(iv) The item (3) in the paragraph (iii) makes the puz-

[2] We obtained $N_e = 5.5 \times 10^9$ for the proton-induced air showers of $E_0 = 10^{19}$ eV, from the figure in Ref. (Nagano et al., 1998), and multiplied it by 10.

Table 3. Air shower size at sea level, expected by the models, for the incident proton of $E_0 = 10^{20}$ eV

	Model-0	Model-1	Model-2	KORSIKA
size*	5.0×10^{10}	6.2×10^{10}	1.1×10^{10}	
ratio to Model-0	(×1.0)	(×1.23)	(×0.22)	
charge exchange	×1.13	×1.13	×1.13	
increasing cross section	×1.18	×1.18	×1.18	
size (expected)**	6.7×10^{10}	8.3×10^{10}	1.5×10^{10}	5.5×10^{10}

* without the processes of increasing cross section and the charge exchange.
** with the processes of increasing cross section and the charge exchange.

zle of extremely high energy cosmic rays more serious.[3] Therefore it may not be irrelevant to say that Model-2 does not describe the highest energy air showers. This examination is important because it is believed that the air shower size is a stable parameter to be unchanged by a slight difference of nuclear interaction characteristics.

Origin of this small size in Model-2 is due to the fact that Model-2, which is the best-fit to the present experimental data, predicts small inelasticity at high energies. For example, the value is as small as 0.2 even at $E_0 = 10^{16}$ eV. (Ohsawa et al., 2000) According to our previous analysis of attenuation mean free paths of hadron and (e, γ) components (Ohsawa and Sawayanagi, 1992), the inelasticity of $< K >= 0.5$ is compatible with the experimental data in the energy region of $10^{14} \sim 10^{16}$ eV.

Appendix A Air shower size

Air shower size is defined as the total number of charged particles in the air shower, among which the electron component is dominant. Therefore we calculate only the electron component for the air shower size. It is given by

$$N_e(E_0, z) = \int_0^z dz' \int_0^\infty dE\, \Pi(E, 0, z - z') \times$$

$$\left[\frac{\phi(s)}{s+1} F_N(E, z') + \xi \frac{\phi(s) + 2b < (1-K)^s >}{s+1} F_\pi(E, z')\right]$$

where $F_N(E, z)$ and $F_\pi(E, z)$ are the number of nucleons and pions with energy E at the depth z. And $\Pi(E_0, 0, z)$ is the number of electrons ($E \geq 0$) under Approximation B.

In the case A we can solve the diffusion equations for nucleons and pions exactly, on the basis of the physical processes described in Section 2, and we have

$$N_e(E_0, z) = \frac{1}{2\pi i} \int \frac{ds}{s(s+1)} \left(\frac{E_0}{\epsilon}\right)^s L(s) \sqrt{s} K_{1,0}(s, -s)$$

$$\times \phi(s) \left[\frac{e^{\mu_N(s) z} - e^{\xi_0 \lambda_1(s) z}}{\mu_N(s) - \xi_0 \lambda_1(s)} + \xi \frac{\phi(s) + 2b < (1-K)^s >}{\mu_N(s) - \xi \mu_\pi(s)} \right.$$

$$\left. \left\{ \frac{e^{\mu_N(s) z} - e^{\xi_0 \lambda_1(s) z}}{\mu_N(s) - \xi_0 \lambda_1(s)} - \frac{e^{\xi \mu_\pi(s) z} - e^{\xi_0 \lambda_1(s) z}}{\xi \mu_\pi(s) - \xi_0 \lambda_1(s)} \right\} \right]$$

where z is measured in the unit of λ_N. (*i.e.*, $\xi = \lambda_N / \lambda_\pi$, $\xi_0 = \lambda_N / X_0$) The integration is a complex one, originated from the inverse Mellin transformation. The first line is related to the cascade functions, and the second and the third are to the π^0 production by nucleons and pions.

The terms $\mu_N(s)$, $\xi \mu_\pi(s)$ and $\xi_0 \lambda_1(s)$ are related to the attenuation of nucleons, pions and electrons, respectively.

$$\mu_N(s) = -1 + < (1-K)^s >$$

$$\mu_\pi(s) = -1 + (1-b) < (1-K)^s > + \phi(s)$$

$$\lambda_1(s) = \text{(by the cascade theory)}$$

where $\phi(s)$ is the Mellin transform of the energy distribution of the produced pions (eq.(2)),

$$\phi(s) = \int_0^1 x^s dx\, \varphi(E_0, E) \qquad (x = \frac{E}{E_0}),$$

and $< (1-K)^s >$ is given by

$$< (1-K)^s >= \int_0^1 (1-K)^s dK = \frac{1}{s+1}$$

[3] The air showers with energy exceeding the GZK cut-off.

References

J.N. Capdevielle et al., Preprint of Kernforschungszentrum Karlsruhe KfK 4998 (1992).

M.N. Dyakonov et al., Proc. 20th Int. Cosmic Ray Conf. (Moscow) Vol.6 (1987) 147.

T.K. Gaisser et al, Rev. Mode. Phys. 50 (1978) 859.

T. Hara et al., Phys. Rev. Lett. 50 (1983) 2058.

M. Nagano et al., Preprint of Forschungszentrum Karlsruhe, FZKA 6191 (1998).

R.A. Nam et al., Proc. 18th Int. Cosmic Ray Conf. (Bangalore) Vol.5 (1983)336.

A. Ohsawa, K. Sawayanagi, Phys. Rev. D49 (1992) 3128-3133.

A. Ohsawa, E.H. Shibuya and M. Tamada, to appear in Phys. Rev. D; in this proceedings.